

A Letter of Intent to the Jefferson Lab PAC43

Search for Hybrid Baryons with CLAS12 in Hall B

Annalisa D'Angelo,^{1,2} Ilaria Balossino,¹¹ Luca Barion,¹¹ Marco Battaglieri,³ Vincenzo Bellini,¹² Volker Burkert,⁴ Simon Capstick,⁵ Daniel Carman,⁴ Andrea Celentano,³ G. Ciullo,¹¹ Marco Contalbrigo,¹¹ Volker Credé,⁵ Raffaella De Vita,³ E. Fanchini,³ Gleb Fedotov,⁶ A. Filippi,¹⁰ Evgeny Golovach,⁶ Ralf Gothe,⁷ Boris S. Ishkhanov,^{6,13} Evgeny L. Isupov,⁶ Valeri P. Koubarovski,⁴ Lucilla Lanza,² P. Lenisa,¹¹ Francesco Mammoliti,¹² Victor Mokeev,^{4,6} A. Movsisyan,¹¹ Mikhail Osipenko,³ Luciano Pappalardo,¹¹ Marco Ripani,³ Allesando Rizzo,² Jan Ryckebusch,⁸ Iuliia Skorodumina,^{7,13} Concetta Sutera,¹² Adam Szczepaniak,^{9,4} Mauro Taiuti,³ M. Turisini,¹¹ Maurizio Ungaro,⁴ and Veronique Ziegler⁴

¹*INFN, Sezione di Roma Tor Vergata, 00133 Rome, Italy*

²*Universita' di Roma Tor Vergata, 00133 Rome Italy*

³*INFN, Sezione di Genova and Dipartimento di Fisica, Universita' di Genova, 16146 Genova, Italy*

⁴*Thomas Jefferson National Accelerator Facility, Newport News, Virginia 23606, USA*

⁵*Florida State University, Tallahassee, Florida 32306, USA*

⁶*Skobeltsyn Institute of Nuclear Physics, Lomonosov Moscow State University, 119234 Moscow, Russia*

⁷*University of South Carolina, Columbia, South Carolina 29208, USA*

⁸*Gent University, Gent, Netherland*

⁹*Indiana University, Nuclear Theory Center, Bloomington, Indiana*

¹⁰*INFN, Sezione di Torino, Torino, Italy*

¹¹*INFN Ferrara e Università di Ferrara, Italy*

¹²*INFN, Sezione di Catania, Catania, Italy*

¹³*Physics Department at Lomonosov Moscow State University, Leninskie Gory, Moscow 119991, Russia.*

(Dated: May 17, 2015)

We plan to submit a proposal to an upcoming Jefferson Lab Program Advisory Committee with the aim to launch an experimental program that will utilize the CLAS12 detector system in Hall B to study the s-channel excitation of baryons with dominant gluonic admixtures (hybrid baryons). The experiment will use electron beams with energies of 6.6, 8.8, and 11 GeV impinging upon a liquid hydrogen target in the CLAS12 center. Scattered electrons will be detected in an angle range of 2.5° to 4.5° in the Forward Tagger and for angles greater than 6° in the CLAS12 Forward Detector. At the requested beam energies, the mass range up to 3.5 GeV over a Q^2 range of 0.05 to 2.5 GeV² will be covered. Due to the high electron rate at the very forward polar angles, additional constraints on the hadronic final state will be built into the CLAS12 trigger system to reduce the recorded event rate to a maximum of 20 kHz.

Contents

I. Introduction	3
II. Theoretical Studies	3
A. Model projections	3
B. Lattice QCD predictions	4
C. Hadronic couplings	5
D. Electromagnetic couplings	6
III. Experimental aspects	7
A. The CLAS12 detector	7
B. The Forward Tagger	7
IV. Simulations	7
A. Event generator for $ep \rightarrow ep\pi^+\pi^-$	7
B. Acceptance estimates for $ep \rightarrow ep\pi^+\pi^-$	8
C. Resolution in hadronic mass reconstruction and background estimation	10
D. Summary of experimental condition study	12
E. The $K\Lambda$ and $K\Sigma^0$ event generator	13
F. Acceptances for $ep \rightarrow e'pK^+\Lambda$	13
G. Count rates from $K^+\Lambda$	19
H. Expected event rates	20
V. Data Analysis	20
A. Event selection	20
B. Event reconstruction	20
C. Extracting differential cross sections and normalized yields	23
D. Partial wave analysis	23
E. Strategies for identifying Hybrid Baryons	23
VI. Other topics in light-quark baryon spectroscopy that are addressed with this LOI	24
VII. Beamtime estimate	24
VIII. Summary	25
IX. Planned Monte-Carlo studies for hybrid baryon manifestation in exclusive KY electroproduction	26
X. Appendix A	29
References	31

I. INTRODUCTION

The ongoing program at Jefferson Lab and several other laboratories to study the excitation of nucleons in the so-called nucleon resonance region with real photon and with electron beams has been very successful. Although only a fraction of the data taken during the CLAS run groups g8, g9, g11, and g12 have been analyzed and published, the published data have allowed for very significant advances in light-quark baryon spectroscopy, and led to strong evidence of several new nucleon excitations as listed in the PDG review of 2014 [1]. These discoveries were possible due to the very high meson production rates recently obtained for energy-tagged photoproduction processes. Furthermore, the use of meson electroproduction has led to completely new insights into the nature of several prominent resonant baryons, e.g. the so-called Roper resonance $N(1440)\frac{1}{2}^+$. This state defied an explanation of its properties, such as mass, transition amplitudes, and transition form factors within the constituent quark model (CQM). The analyses of the new electroproduction data were crucial in dissecting its complex structure and providing a qualitative and quantitative explanation of the space-time evolution of the state [2]. The Roper was also considered as a candidate for the lowest mass hybrid baryon [3]. It was only through the meson electroproduction data that this possibility could be dismissed [4, 5].

The theory of the strong interactions, QCD, not only allows for the existence of baryons with dominant gluonic contributions (hybrid baryons), but Lattice QCD calculations now predict several baryon states with dominant gluonic admixture to the wave function, and with the lowest mass hybrids approximately 1.3 GeV above the nucleon ground state of 0.94 GeV, i.e. in the range $W = 2.2 - 2.3$ GeV. In the meson sector, exotic states (hybrid mesons) are predicted with quantum numbers that cannot be obtained in a pure $q\bar{q}$ configuration. The selection of mesons with such exotic quantum numbers provides a convenient way to identify candidates for gluonic mesons. In contrast to the meson sector hybrid baryons have quantum numbers that are also populated by ordinary excited 3-quark states. Hybrid baryons hence mix with these 3-quark excited states or with dynamically generated states making the identification of gluonic baryons more difficult. An important question is therefore: How can we distinguish gluonic excitations of baryons from their ordinary quark excitations? Another question is the mass range in which we may expect hybrid baryons to occur.

Mapping out the nucleon spectrum and the excitation strengths of individual resonances is a powerful way to answer a central question of hadron physics: "What are the effective degrees of freedom as the excited states are probed at different distance scales?". Previous analyses of meson electroproduction have shown to be most effective in providing answers in several cases of excited states: $\Delta(1232)\frac{3}{2}^+$, $N(1440)\frac{1}{2}^+$, $N(1520)\frac{3}{2}^-$, $N(1535)\frac{1}{2}^-$, $N(1680)\frac{5}{2}^+$, and $N(1675)\frac{5}{2}^-$. The experimental program outlined in this Letter-of-Intent is meant to vastly improve upon the available information and extend the reach of meson electroproduction to cover the full nucleon resonance mass range up to 3.5 GeV and a larger low Q^2 range from 0.05 to 2 GeV². In conjunction with experiment E12-09-003, which focusses on the highest Q^2 , as well as E12-06-108A, which explores $K^+\Lambda$ production, the proposed experiment will provide a complete program of nucleon resonance electroexcitation.

II. THEORETICAL STUDIES

A. Model projections

In an extension of the MIT bag model, gluonic excitations of the nucleon, to states where a constituent gluon in the lowest energy transverse electric mode combines with three quarks in a color octet state to form a colorless state in the mass range of 1.600 ± 0.100 GeV, have been broadly discussed since 1983 [3].

The gluon flux-tube model applied to hybrid baryons [6, 7] came up with similar quantum numbers of the hybrid states, but predicted considerably higher masses than the bag model. For the lowest mass flux-tube hybrid baryon a mass of 1.870 ± 0.100 GeV was found. In all cases the lowest mass hybrid baryon was predicted as a $J^P = 1/2^+$ state, i.e. a nucleon-like or Roper-like state. Hybrid baryons were also discussed in the Large N_c approximation of QCD for heavy quarks [8], which also led to the justification of the constituent glue picture used in the models. The high energy behavior of hybrid baryons was discussed in [9]. However, in contrast to hybrid meson production, which has received great attention both in theory and in experiments, the perceived difficulties of isolating hybrid baryon states from ordinary quark states led this part of the field to remain dormant for a decade.

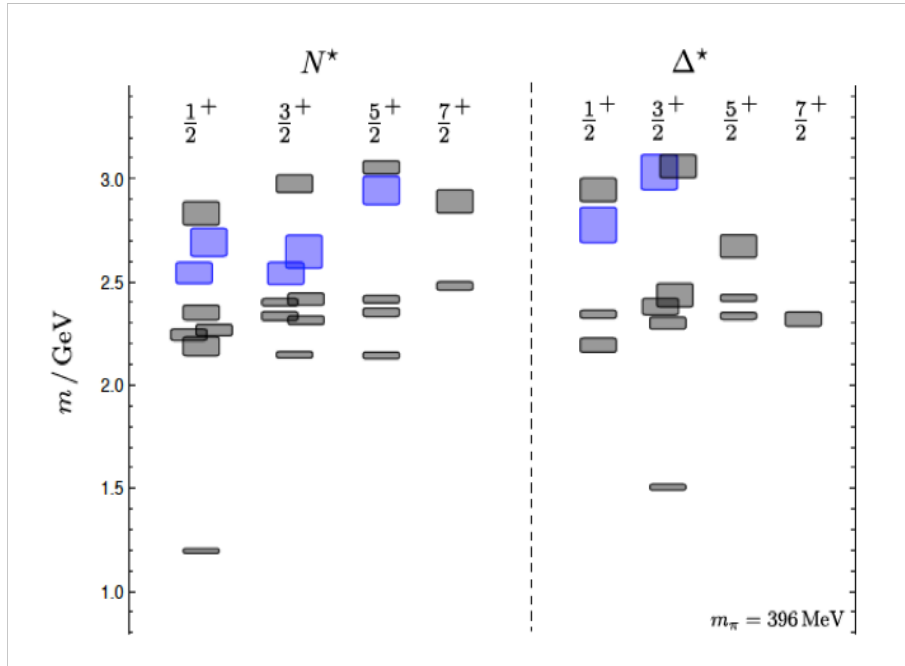


FIG. 1: The light-quark baryon spectrum predicted in Lattice QCD at a pion mass of 396 MeV. The blue shaded boxes indicate states with dominant gluonic contributions. Note that both the mass of the nucleon ground state and of the $\Delta(1232)$ are shifted by nearly 300 MeV to higher masses.

B. Lattice QCD predictions

The first quenched calculations on the lattice came in 2003 [10], when the lowest gluonic 3-quark hybrid system was projected at a mass of 1 GeV above the nucleon mass, placing the lowest hybrid baryon at a mass around 2 GeV. The first LQCD calculation of the full light-quark baryon spectrum with unquenched quarks occurred in 2012 that included the projections of the hybrid nucleon N_G states and hybrid Δ_G states [11]. Figure 1 shows the projected light quark baryon spectrum in the lower mass range.

At the pion mass of 396 MeV used in this projection, the prediction for the nucleon mass is shifted by nearly 300 MeV to higher masses. In the following we take this shift into account by subtracting 300 MeV from the masses of the excited states in Fig. 1. As stated in [11], the lowest hybrid baryons, shown in Fig. 1 in blue, were identified as states with leading gluonic contributions. If hybrid baryons are not too wide, we might expect the lowest hybrid baryon to occur at masses of about 1.3 GeV above the ground state, i.e. in a mass range of 2.2 - 2.3 GeV, a few hundred MeV above the band of radially excited $J^P = \frac{1}{2}^+$ 3-quark nucleon excitations of isospin 1/2 and thus possibly well separated from other states.

In this computation the lowest $J^P = \frac{3}{2}^+$ gluonic states are nearly mass degenerate with the corresponding $J^P = \frac{1}{2}^+$ gluonic states generating a glue-rich mass range of hybrid nucleons. If these projections hold up with LQCD calculations using near physical pion masses, one should expect a band of the lowest mass hybrid baryon states with spin-parity $\frac{1}{2}^+$ and $\frac{3}{2}^+$ to populate a relatively narrow mass band of 2.2 - 2.5 GeV. Note, that these states fall into a mass range where no 3-quark nucleon excitations are predicted to exist from these calculations. The corresponding negative parity hybrid states, which are expected to occur at much higher masses, are not included in this graph, and are not further considered here; although they may be subject of analysis, should they appear within the kinematic range covered by this LoI.

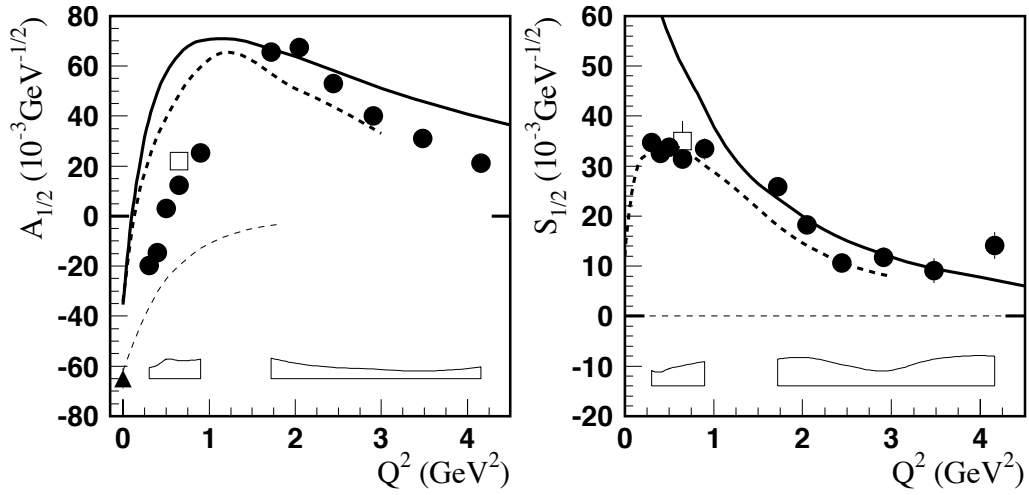


FIG. 2: Electrocoupling amplitudes of the Roper resonance $N(1440)_{\frac{1}{2}}^{+}$. The thin dashed lines are the constituent quark-gluon model predictions for the gluonic Roper

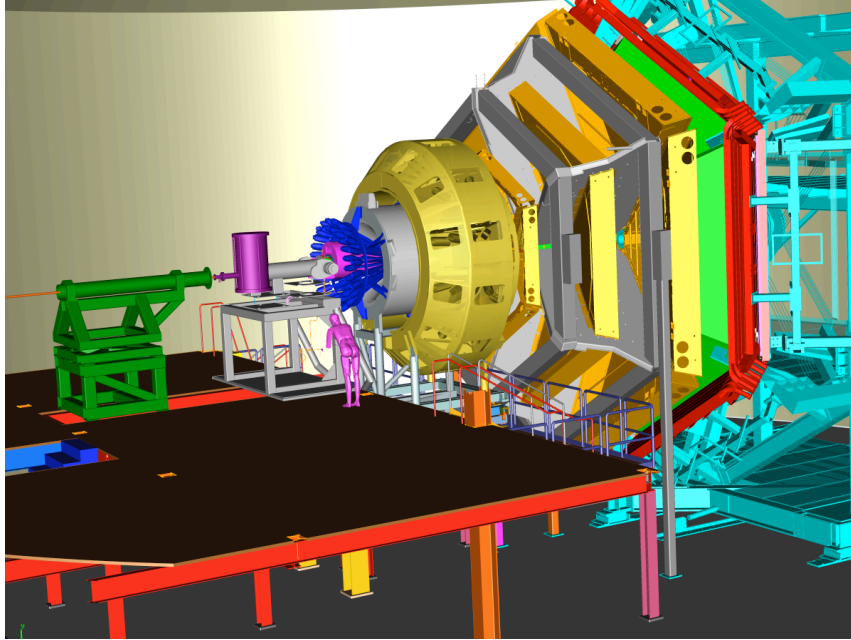


FIG. 3: The CLAS12 detector has high hermeticity and high multiplicity reconstruction, can run at high luminosity ($L > 10^{35} \text{ cm}^{-2} \text{ s}^{-1}$), and is best suited to carry out the proposed experiment.

C. Hadronic couplings

Very little is known about possible hadronic couplings of hybrid baryons. One might expect an important role for final states with significant gluonic admixture, e.g. $B_G \rightarrow N\eta'$ [12], or final states containing $s\bar{s}$ contributions due to the coupling $G \rightarrow s\bar{s}$, e.g. $B_G \rightarrow K^+\Lambda$, $B_G \rightarrow N^*(1535)\pi \rightarrow N\eta\pi$, $B_G \rightarrow N\pi\pi$, $B_G \rightarrow \phi(1020)N$, and $B_G \rightarrow K^*\Lambda$. Quark-model estimates of the hadronic couplings would be helpful in selecting the most promising final state for the experimental evaluation. As long as such estimates are not available we will use a range of assumptions on the

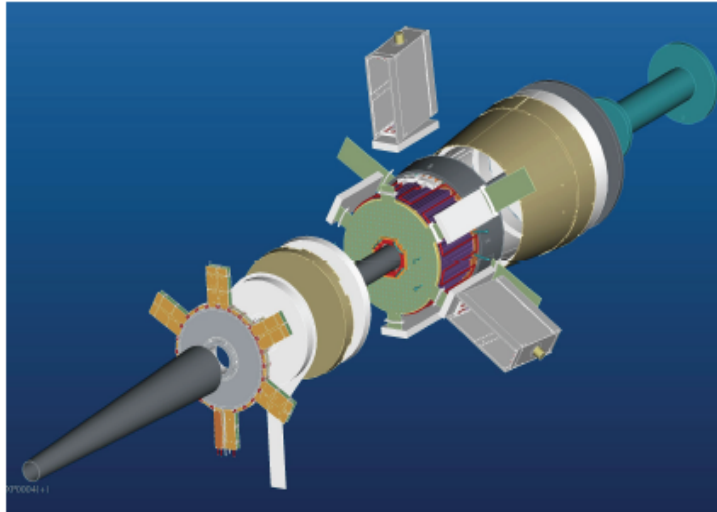


FIG. 4: The Forward Tagger (FT) system. The FT provides electron and high energy photon detection in a range of polar angles $\theta_e = 2.5^\circ - 4.5^\circ$, and will be fully integrated into the operation of CLAS12.

hadronic couplings to estimate the sensitivity required for definitive measurements. Assuming hadronic couplings of a few percent in the less complex final states, e.g. $K^+\Lambda$, $K^*\Lambda$, or $N\pi\pi$, we should be able to identify these states and proceed to experimentally establish their electromagnetic couplings and Q^2 dependences.

D. Electromagnetic couplings

Electromagnetic couplings have been studied within a non-relativistic constituent quark-gluon model, but only for two possible hybrid states, the Roper $N_G(1440)\frac{1}{2}^+$ and the $\Delta_G(1600)\frac{3}{2}^+$. In reference [14] the photoexcitation of the hybrid Roper resonance $N(1440)\frac{1}{2}^+$ was studied, and in reference [15] the electroproduction transition form factors of a hybrid Roper state were evaluated. The latter was essential in eliminating the Roper resonance as a candidate for a hybrid state, both due to the transverse helicity amplitude and its Q^2 dependence and the prediction of $S_{1/2}(Q^2) = 0$ at all Q^2 . It also showed that a hybrid Roper transition amplitude $A_{1/2}$ should behave like the $A_{1/2}$ of the ordinary $\Delta(1232)$. Clearly the $S_{1/2}$ behaves differently and the $A_{3/2}$ does not exist for the Roper. Recent measurements of the electrocoupling transition amplitudes are shown in Fig. 2. Both amplitudes exhibit a Q^2 dependence that is distinctively different from the hybrid baryon prediction. Especially the scalar amplitude $S_{1/2}(Q^2)$ was found to be large while it is predicted to be suppressed in leading order for the lowest mass $\frac{1}{2}^+$ hybrid state.

The aforementioned predictions should apply to each lowest mass hybrid state with $J^P = \frac{1}{2}^+$ and $\frac{3}{2}^+$. One may ask about the model-dependence of this prediction. The transverse amplitude has model sensitivity in its Q^2 dependence and it depends on model ingredients, however, there are no ordinary 3-quark model predictions that would come even close to the predictions of the hybrid quark-gluon model. The radial excitation of the Roper resonance gives a qualitatively different prediction for $A_{1/2}(Q^2)$ compared to the hybrid excitation, where the 3-quark component remains in the ground state with only a spin-flip occurring (just as for the $N - \Delta(1232)$ transition). The suppression of the longitudinal coupling is a property of the γqG vertex and is largely independent of specific model assumptions.

The other state, $\Delta(1600)\frac{3}{2}^+$, was considered as a candidate for the lowest mass gluonic Δ_G . A result similar to the one for the hybrid Roper is found in [15] for a hybrid $\Delta_G(1600)\frac{3}{2}^+$, i.e. a fast falling $A_{1/2}(Q^2)$ and $S_{1/2}(Q^2) \approx 0$. The amplitudes at the photon point are not inconsistent with the ordinary 3-quark model calculation but are inconsistent with the hybrid baryon hypothesis. On the other hand this result is also in line with the expectation that the lowest mass hybrid states should have considerably higher masses than the first radially excited quark states. Note that there are currently no experimental results for the Q^2 dependence of the $A_{1/2}$ and $S_{1/2}$ amplitudes of this state.

III. EXPERIMENTAL ASPECTS

A. The CLAS12 detector

The experimental program will use the CLAS12 detector, shown in Fig. 3, for the detection of the hadronic final state. CLAS12 consists of a Forward Detector (FD) and the Central Detector (CD). The Forward Detector is comprised of six symmetrically arranged sectors defined by the six coils of the toroidal superconducting magnet. Charged particle tracking is provided by a set of 18 drift chambers with a total of 36 layers in each sector. Additional tracking at $5^\circ - 35^\circ$ is achieved by a set of 6 layers of micromesh gas detectors (micromegas) immediately downstream of the target area and in front of the High-Threshold Cherenkov counter (HTCC). Particle identification is provided by time-of-flight information from two layers of time-of-flight detectors (FTOF). Electron, photon, and neutron detection are provided by the triple layer electromagnetic calorimeter, PCAL, EC(inner), and EC(outer). The heavy gas Cherenkov Counter (LTCC) provides separation of high momentum pions from kaons and protons. The Central Detector consists of 6-8 layers of silicon strip detectors with stereo readout, 6 layers of micromegas, arranged as a barrel around the target, 48 scintillator bars to measure the particle flight time from the target (CTOF), and a central neutron detector. Further details on all CLAS12 components (magnets, detectors, data acquisition, software) may be obtained from Ref. [13].

A polarized electron beam will be scattered off a liquid hydrogen target. The scattered electrons will be detected in the the Forward Detector of CLAS12 for scattering angles greater than about 6° and in Forward Tagger for angles from 2.5° to 4.5° , which allows us to cover the Q^2 range of interest between 0.05 and 2 GeV². Charged hadrons will be measured in the full range from 6° to 130° . At an operating luminosity of $L = 10^{35} \text{ cm}^{-2}\text{s}^{-1}$ hadronic rates of $5 \times 10^6 \text{ s}^{-1}$ are expected.

B. The Forward Tagger

An essential component of the hadron spectroscopy program with CLAS12 is the Forward Tagger (FT) shown in Fig 4. The FT uses a high resolution crystal calorimeter composed of 324 lead-tungstate crystals to measure the scattered electrons in the polar angle range from 2.5° to 4.5° and with full coverage in azimuthal angle. The calorimeter measures electron and photon energies with an energy resolution of $\sigma(E)/E \leq 0.02/\sqrt{E(\text{GeV})} + 0.01$. The fine granularity of the calorimeter also provides good polar angle resolution. A two-layer tiled scintillator hodoscope is located in front of the calorimeter for the discrimination of photons. An additional four-layer micromegas tracker, located in front of the hodoscope, will be used for precise electron tracking information. Electron detection in the FT will allow us to probe the crucial Q^2 range where hybrid baryons may be identified due to their fast dropping $A_{1/2}(Q^2)$ amplitude and the suppression of the scalar $S_{1/2}(Q^2)$ amplitude.

Construction of the FT is currently underway at INFN/Genova (Italy), CEA/Saclay (France), and the University of Edinburgh (UK). The FT is expected to be ready for shipment to Jefferson Lab and installation into CLAS12 in the Fall of 2015.

IV. SIMULATIONS

In order to account realistically for the acceptance of the processes we want to study, two event generators were developed for the processes $ep \rightarrow e'K^+\Lambda$ (and $\Lambda \rightarrow p\pi^-$) and $ep \rightarrow e'p\pi^+\pi^-$, respectively. Both reactions have four charged tracks in the final state and the event pattern coming from resonance decays may be quite similar. To the degree possible the event generators have been tuned to existing data, mostly from CLAS. However, extrapolations to high W and very small Q^2 have been necessary, since no prior data exist. The generator for $ep \rightarrow e'p\pi^+\pi^-$ has been initially used to determine the most efficient configuration for beam energy and torus magnet setting in terms of field polarity and current.

A. Event generator for $ep \rightarrow ep\pi^+\pi^-$

The Monte Carlo simulation of the $\pi^+\pi^-p$ exclusive electroproduction was carried out in the range of invariant masses of the final hadron system W from the two-pion production threshold to 3 GeV and at photon virtualities Q^2 from 0.05 GeV² to 2.0 GeV². The GENEV event generator that employs five-fold differential cross sections from the JM05-version [21–23] of the meson-baryon model JM was used. The JM05 model version incorporates reaction

mechanisms that are sufficient for a realistic simulation of the event distributions in the reaction phase space. The generated events in the Q^2 , W plane are shown in Fig. 5.

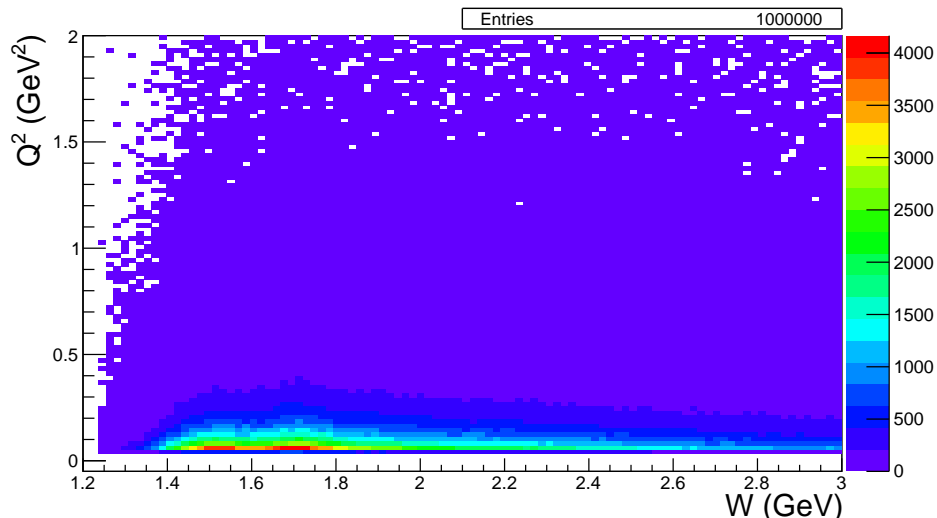


FIG. 5: Q^2 versus W distribution for the generated $\pi^+\pi^-p$ events with an electron beam energy of 6.6 GeV. The GENEV event generator based on JM05 [21–23] was used to generate 10^6 events.

The established GENEV version of the two-pion event generator is written in FORTRAN and has several limitations. It employs $\pi^+\pi^-p$ differential cross sections from the older JM05 version of the JM model [21–23]. During the past several years the model was further developed [31] and significantly improved. Furthermore, the two-pion part of the GENEV is only applicable up to 2 GeV in W and from 0.3 GeV^2 in Q^2 , and therefore excludes most of the region of interest (high W and low Q^2), where it uses simple interpolations. An effort to develop a new event generator for the simulation of the $\pi^+\pi^-p$ electroproduction off protons has been initiated for this Letter-of-Intent. The new event generator employs the 5-fold differential cross sections from the recent version of the JM15 model fit to all results on charged double pion photo- and electroproduction cross sections from CLAS (both the published and preliminary [25–28]). The output format is compatible with the new CLAS12 reconstruction software.

In the W range from 1.4 GeV to 1.8 GeV and Q^2 from 0.65 GeV^2 to 1.3 GeV^2 the new generator successfully reproduces the available integrated and single differential 2π cross sections [25].

The quality of the description is illustrated on the left side in Fig. 6 for two intermediate Q^2 bins (0.65 GeV^2 in green and 0.95 GeV^2 in blue) and for a quasi-real Q^2 (0.0015 GeV^2 in black) in comparison with the available data [16]. In order to extend the kinematical coverage toward extremely low Q^2 , the integrated cross sections of 2π photoproduction were used [28]. The resulting Q^2 dependence of the total cross section, is shown in the right plot of Fig. 6. The next step of the event generator development will be an extension of the kinematical coverage to W up to 2.5 GeV.

B. Acceptance estimates for $ep \rightarrow ep\pi^+\pi^-$

For the event reconstruction a simplified version of the CLAS12 event reconstruction software, the so-called FASTMC routine, was employed to filter the generated events for acceptance. This routine accounts for the detector fiducial areas and provides smearing over the final particle angles and momenta. The accepted events are shown in Fig. 7 and are plotted in the Q^2 versus W plane. The different panels show distributions for reconstructed $\pi^+\pi^-p$ events at various beam energies. The torus current was set to +3375 A, which forces negatively charged particles to bend towards the beam line. The areas of zero acceptance seen in the plots represent the gap between the Forward Tagger and the minimum polar angle accepted in CLAS12 for inbending particles. For the hybrid baryon search the area of small photon virtuality is of particular interest. The size of the gap depends on the torus current setting and the momentum of the scattered electrons. For a negative Torus current, i.e. outbending electrons, the gap is simply given by the geometrical acceptance of CLAS12 and is largely independent of the particle momentum, while for inbending particles the acceptance depends on scattering angle, particle momentum, and magnetic field strength.

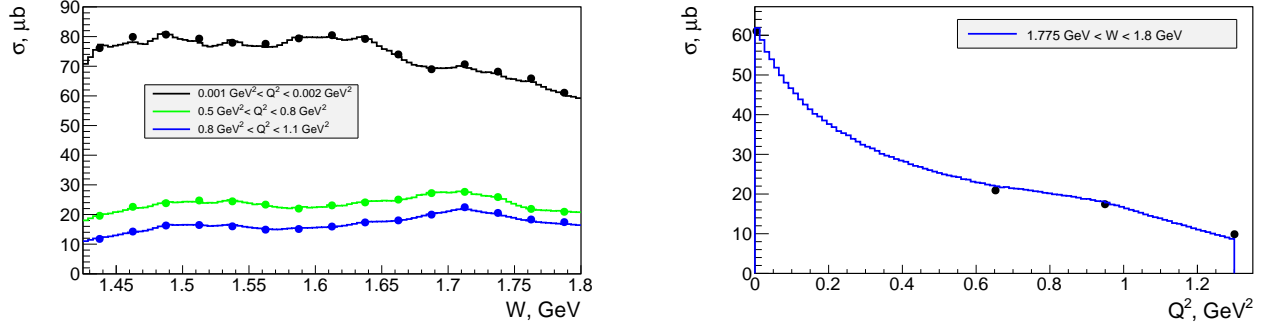


FIG. 6: Comparison between event distributions of the new two-pion event generator (curves) with the integrated cross sections from JM15 [24] and data [16] (points). Left plot shows the W dependence of the total cross section for three Q^2 bins in comparison with the model and data for the corresponding three Q^2 points at 0, 0.65, and 0.95 GeV^2 . Right plot shows a typical Q^2 -dependence example of the total cross section for one W bin in comparison with JM15 at $W = 1.7875 \text{ GeV}$. The point at $Q^2 = 0$ corresponds to still unpublished CLAS photoproduction data [28], while the following three points correspond to data from [25].

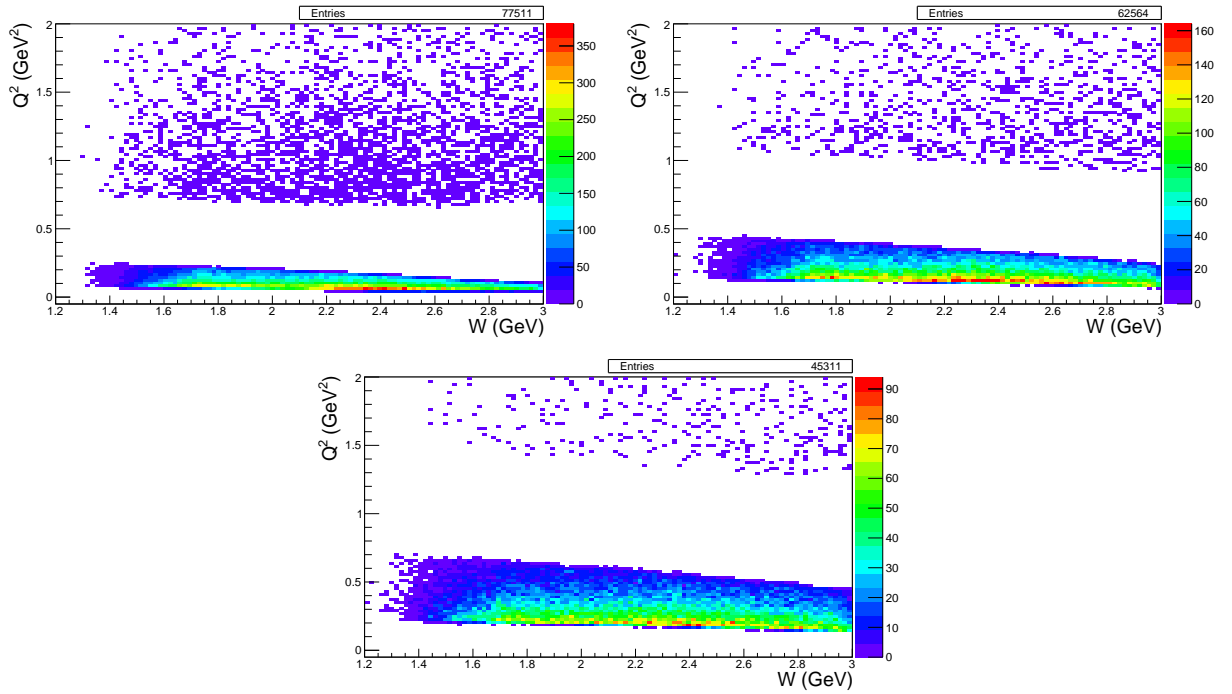


FIG. 7: Q^2 versus W distributions for the reconstructed $\pi^+\pi^-p$ events (all particles in final state are registered). Top left, right, and bottom plots correspond to 6.6 GeV, 8.8 GeV, and 11 GeV beam energies, respectively. The torus current is set to + 3375 A.

The acceptance for electron scattering angles from 2.5° to 4.5° , which is covered by the FT, is independent of the torus current settings. In order to cover photon virtualities as low as 0.05 GeV^2 measurements with 6.6 GeV electron beam energy are required. The minimal Q^2 values for reconstructed events increase up to 0.13 GeV^2 and 0.2 GeV^2 for beam energies of 8.8 GeV and 11 GeV, respectively. A simulated $ep \rightarrow e'p\pi^+\pi^-$ event in CLAS12 is shown in Fig. 8.

With a beam energy of 6.6 GeV, the influence of the magnetic field direction on the accessible kinematical coverage for $\pi^+\pi^-p$ electroproduction was further studied. The Q^2 versus W distributions for reconstructed $\pi^+\pi^-p$ events are shown in Fig. 9 for two opposite polarities of the torus current, +3375 A and -3375 A, which correspond to the maximum expected currents. A wide area of zero acceptance for the normal (+3375 A) direction of the magnetic field is clearly seen in Figure 9 (left). Reversing the magnetic field allows us to decrease substantially the inefficient area, as is shown in Fig. 9 (right). Therefore, the reversed magnetic field represents the best configuration for the proposed

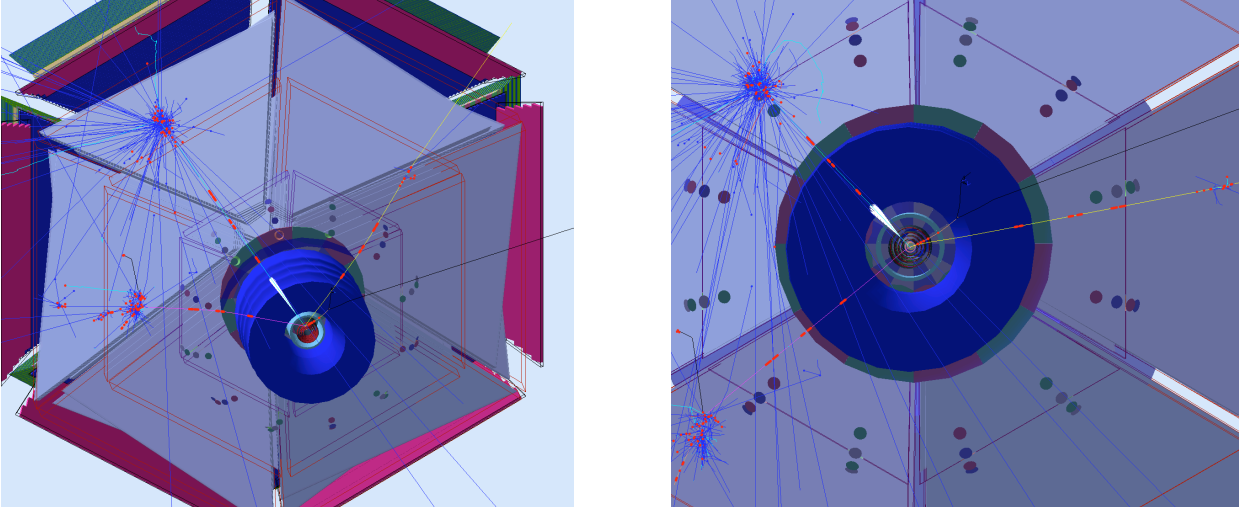


FIG. 8: A Geant4 $ep \rightarrow ep\pi^+\pi^-$ event as seen in CLAS12. The left graph shows the scattered electron (cyan) generating Cherenkov light in the HTCC, leaving track segments in the 3 drift chamber regions, and hits in the FTOF planes and finally shower in the PCAL & EC calorimeters. The two pions π^+ (purple line) and π^- (yellow line) are tracked in the DCs, and leave hits in the FTOFs and calorimeters. The proton (short orange line) is tracked at large angles inside the solenoid magnet in the four SVT regions, and leaves hits in the CTOF. The right panel shows a close-up view of the same event from a different angle. The torus magnet is at 50% of full current.

experiment, as well as for other experiments, for which the area of small photon virtualities is of particular interest.

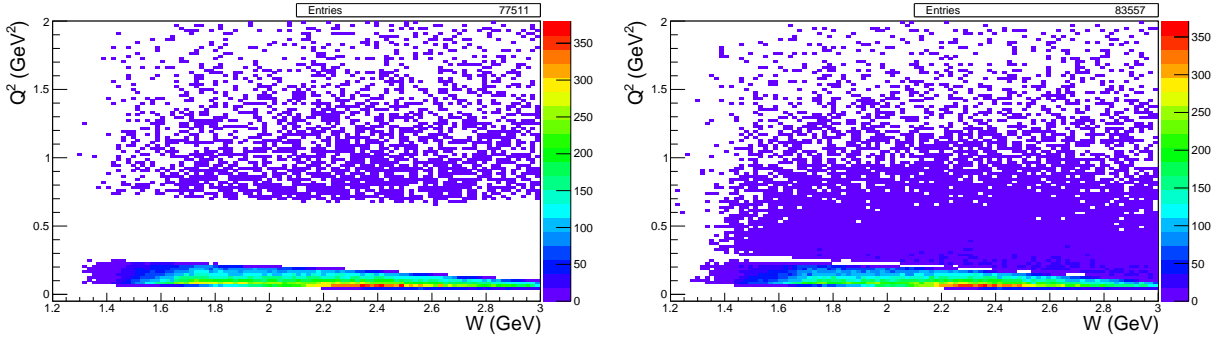


FIG. 9: Q^2 versus W distributions for reconstructed $\pi^+\pi^-p$ events (all particles in final state are registered) for the torus currents +3375 A (left) and -3375 A (right). The reversed magnetic field closes the gap between the Forward Tagger and CLAS12.

We also examined the evolution of counting rates as a function of the magnetic field strength. The 2D Q^2 versus W distributions for the accepted $\pi^+\pi^-p$ events are shown in Fig. 10 for the torus currents, -3375 A (left) and -1500 A (right), that correspond to the full and less than half strength magnetic fields for the CLAS12 detector. Comparing the reconstructed event rates shown in Fig. 10, we expect the counting rate to increase by almost a factor of two at half strength of the magnetic field, because of the improved acceptance for the detection of all three $\pi^+\pi^-p$ particles in the final state and the scattered electron. While the particle momentum resolution will be negatively affected by a lower field, a 50% to 60% value of the CLAS12 torus field is a good compromise between good momentum resolution and large acceptance for the proposed measurement.

C. Resolution in hadronic mass reconstruction and background estimation

The hadronic mass resolution is of particular importance in studies of excited nucleon states, since this quantity determines the ability to reliably extract the resonant contributions in exclusive cross sections. For a credible sep-

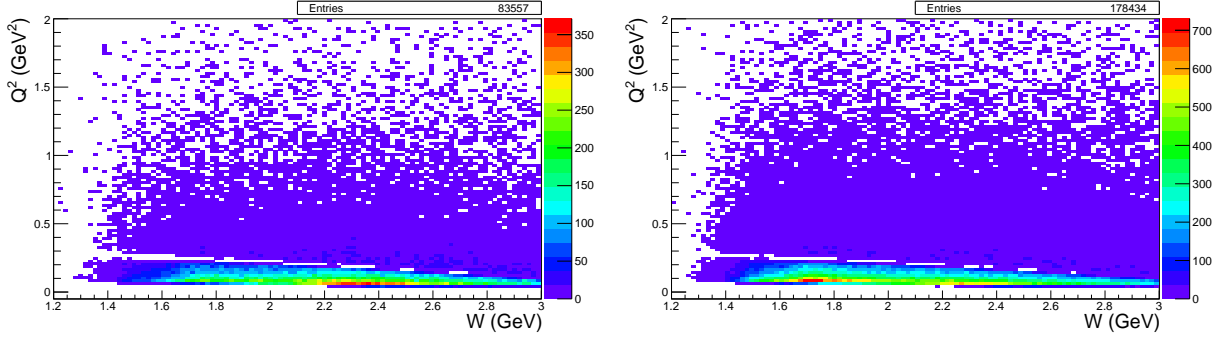


FIG. 10: Q^2 versus W distributions for reconstructed $\pi^+\pi^-p$ events at 6.6 GeV beam energy (all final state particles are registered) with torus currents: -3375A (left) and -1500A (right). With lower torus current significantly more events are reconstructed.

ration between the resonant and the non-resonant contributions the resolution over W should be much smaller than the N^* decay width. Typical values for the decay widths of nucleon resonances with masses > 2.0 GeV are in a range from 250 to 400 MeV. Hence a mass resolution of ≈ 25 MeV is sufficient for the reliable isolation of contributions from hybrid-baryons that are expected in the mass range from 2.0 to 3.0 GeV. The resolution in W for the reconstructed $\pi^+\pi^-p$ events was studied in the following way. For each reconstructed event we compute the difference between the exact W_{gen} and the reconstructed W_{rec} . We compare two different ways of determining the invariant mass of the final hadron system: a) from the difference between the four-momenta of the initial and the scattered electrons that is added to the four-momentum of the target proton (electron scattering kinematics) b) from the sum of the four-momenta of the final π^+ , π^- , and proton (hadron kinematics). The reconstructed $W_{gen} - W_{rec}$ event distributions provide the necessary information on the invariant mass resolution.

The aforementioned distributions for the electron scattering and hadron kinematics are shown in Fig. 11. The beam energy is set to 6.6 GeV and torus current to -1500 A. For both ways of determining the W_{rec} value, the resolution over the full W range is better than 25 MeV and sufficient for the separation of resonant/non-resonant contributions. If W_{rec} is computed from the hadron kinematics, the resolution is significantly better than in the case of electron scattering kinematics. However, the hadron kinematics requires the registration of all final hadrons with a detection efficiency much lower than in the inclusive case where the value of W_{rec} is determined from the electron scattering kinematics.

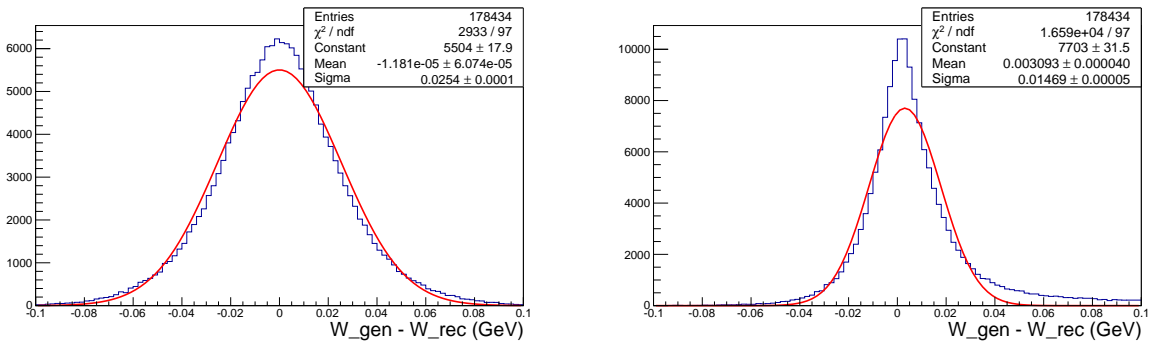


FIG. 11: The $W_{gen} - W_{rec}$ distributions for $\pi^+\pi^-p$ events where W_{rec} is determined by electron scattering (left) and hadron (right) kinematics. See text for explanation of both kinematics.

The studies of charged double pion electroproduction with the CLAS detector [25, 27] demonstrated that the topology, where the final π^- is not detected and its four-momentum is reconstructed from energy-momentum conservation, provides the dominant part of the statistics. Hence topologies in which one of the final pions is not detected will provide the dominant statistics also in the proposed experiment. We are planning to select the $\pi^+\pi^-p$ events by employing exclusivity cuts on the missing mass squared distributions of either the final π^+ or π^- . The contribution from other exclusive channels (exclusive background) to the events within the exclusivity cuts was evaluated in the Monte-Carlo simulation. Most of the exclusive background events come from the $ep \rightarrow e'p'\pi^+\pi^-\pi^0$ channel. Both $\pi^+\pi^-p$ and 3π events were generated with a relative contribution from 3π events of $\approx 9\%$. A phase space distribution is assumed for the 3π events. With this mixture of generated events we reconstructed the $\pi^+\pi^-p$ events and deter-

Energy (GeV)	Current (A)	Eff. all reg.	Eff. π^+ miss (%)	Eff. π^- miss (%)	miss. π^+	miss. π^-	Q_{min}^2	$\sigma(W)$	$\sigma(\sqrt{s})$
11	+3375	4.5					0.2	34	16
11	-3375	4.2					0.2	34	15
11	+1500	8.4					0.2	36	16
11	-1500	8.3					0.2	36	16
8.8	+3375	6.2					0.13	29	16
8.8	-3375	6.1					0.13	29	15
8.8	+1500	12.2					0.13	31	15
8.8	-1500	12.5					0.13	31	16
6.6	+3375	7.8	13.4	12.3	0.21	0.28	0.05	23	15
6.6	-3375	8.4	17.0	12.9	0.21	0.26	0.05	25	14
6.6	+1500	16.0	21.2	21.0	0.14	0.18	0.05	23	15
6.6	-1500	17.8	25.0	21.4	0.23	0.23	0.05	25	15

TABLE I: Comparison of run conditions for the $\pi^+\pi^-p$ channel. The highlighted bottom row represents the optimal run condition for the 6.6 GeV beam energy run.

mined their distribution over the missing mass squared for π^+ and π^- . They are plotted in Fig. 12. The blue curves in Fig. 12 show the 2π event contributions and the green curves represent the 3π event contributions. The exclusivity cuts provide excellent isolation of the $\pi^+\pi^-p$ events with almost negligible contribution from the 3π events.

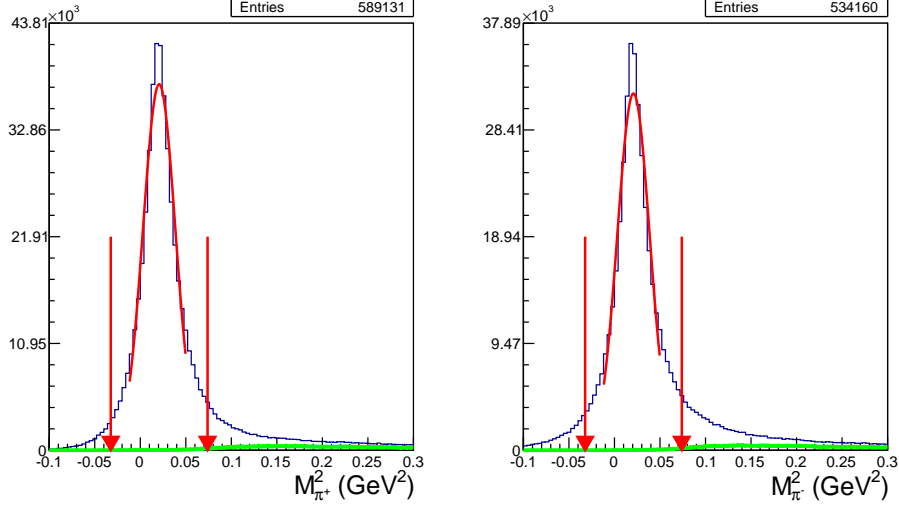


FIG. 12: The reconstructed $\pi^+\pi^-p$ event distributions of the missing masses squared of π^+ (left) and π^- (right) for the generated $\pi^+\pi^-p$ events with an admixture of 9% from 3π events. The contributions from the $\pi^+\pi^-p$ and the $\pi^+\pi^-\pi^0p$ events are shown in blue and green, respectively. The red arrows indicate the applied exclusivity cuts.

D. Summary of experimental condition study

The summary of the run conditions studied in the simulations described above is listed in Table I. The bottom row corresponds to the optimal set-up for the proposed experiment. Whereas the summary of the kinematical coverage in terms of $2D$ plots of ϕ versus θ distributions for the final hadrons is shown in Fig. 13 for all final hadrons detected, a beam energy of 6.6 GeV, and torus current -1500 A. The vertical strips at $\theta = 40^\circ$ in all plots of Fig. 13 correspond to the detector gap between forward and central parts of CLAS12. Since a reversed torus magnetic field was chosen, the low angle area is better populated for negatively charged particles (π^-).

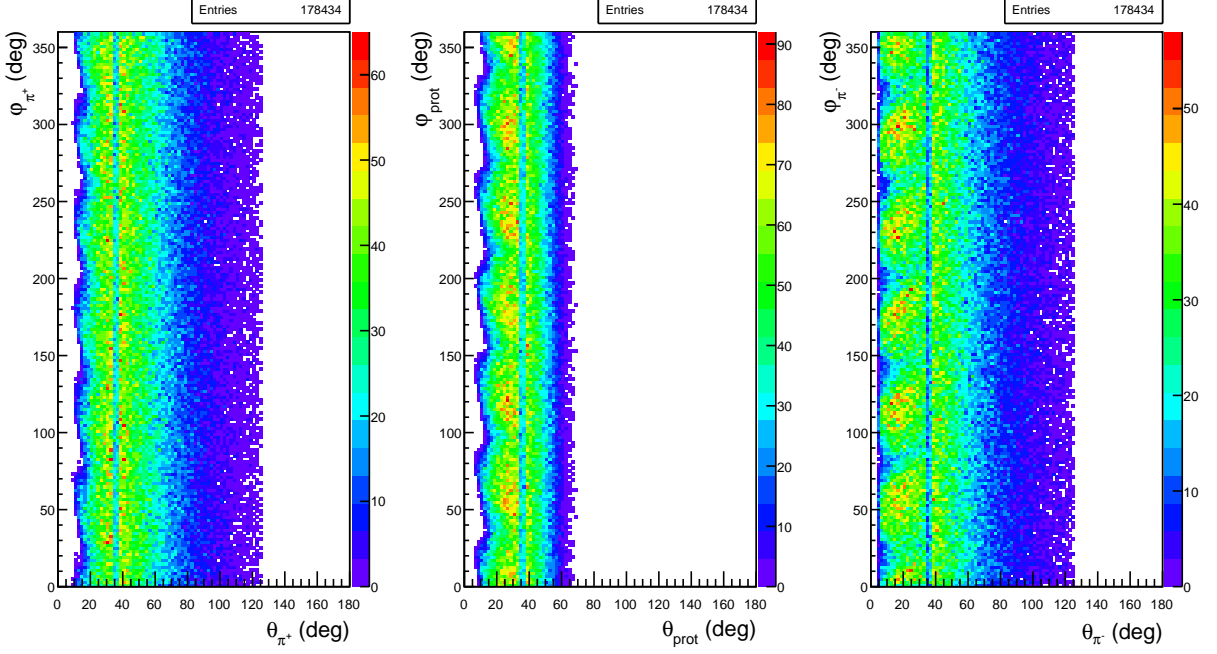


FIG. 13: φ vs θ distributions for the final hadrons: π^+ (left), proton (middle), and π^- (right).

E. The $K\Lambda$ and $K\Sigma^0$ event generator

The $ep \rightarrow e'K^+\Lambda$ event generator is based on model cross section calculations. The models [17] for the $K^+\Lambda$ and [18] for the $K^+\Sigma^0$ channels describe KY electroproduction in the framework of a Regge-plus-resonance approach. Resonance contributions in the s-channel are described with the help of the effective-Lagrangian approach and the background part of the amplitude is modeled in terms of t-channel Regge-trajectory exchange.

A comparison of the fully integrated model cross section with experimental CLAS data is shown in Fig. 14. The cross sections are presented as a function of Q^2 for a given bin in $W = 2.05$ GeV. Differential cross sections in certain bins of Q^2 and W are shown in Figs. 15 and 16. The model reproduces the experimental data for $0.65 \text{ GeV}^2 < Q^2 < 1.5 \text{ GeV}^2$, while it considerably underestimates the cross section for $Q^2 > 1.5 \text{ GeV}^2$. This underestimation is especially notable in the $K^+\Sigma^0$ channel for high Q^2 and low W , see plot corresponding to $Q^2 = 1.8 \text{ GeV}^2$ and $W = 1.73 \text{ GeV}$ in Fig. 16. It does not create any problems since our region of interest is at low Q^2 . We have to rely on the model cross section for $Q^2 < 0.65 \text{ GeV}^2$, as there are no experimental data to compare to. We can see in Figs. 15 and 16 that the model reproduces well the general features of the sharp cross section growth at large $\cos(\theta)$ for $Q^2 > 1.5 \text{ GeV}^2$ and $W > 2.0 \text{ GeV}$.

F. Acceptances for $ep \rightarrow e'pK^+\Lambda$

In Figs. 17 and 18 we compare the angular distributions of all final states particles for an electron beam of 6.6 GeV and for torus currents of +1500 A and the -1500 A. In Fig. 17 we see qualitatively the same behavior as for the $p\pi^+\pi^-$ final state: inbending electrons generated in a W interval from $K^+\Lambda$ threshold at 1.6 GeV to 3.5 GeV and scattering angles $\theta_e \geq 2^\circ$ are detected in CLAS12 starting at about 6.5° with the acceptance opening up towards larger scattering angles. The swirly pattern seen in the accepted protons and K^+ is due to the azimuthal motion of charged tracks in the strong solenoid field that generates a "kick" in azimuth that depends on the production angle and the particle momentum. It should be noted that the particles are not traversing the sectors in this pattern, as the plotted quantities are the values at the production vertex. The pattern for the π^- is different as they have on average much lower momenta and their migration in ϕ is larger and more diffuse. For KY production off hydrogen, the recoil protons are kinematically limited to polar angles of $\leq 65^\circ$. Figure 18 shows the acceptances for out-bending electrons for which the polar angle gap between the FT and CLAS12 is strongly reduced and the azimuthal response is more uniform. As a result, the event acceptance for this configuration is almost a factor 2 larger than for the in-bending field configuration. We also note that for both configurations there exists a polar-angle band from 35° to 40° where

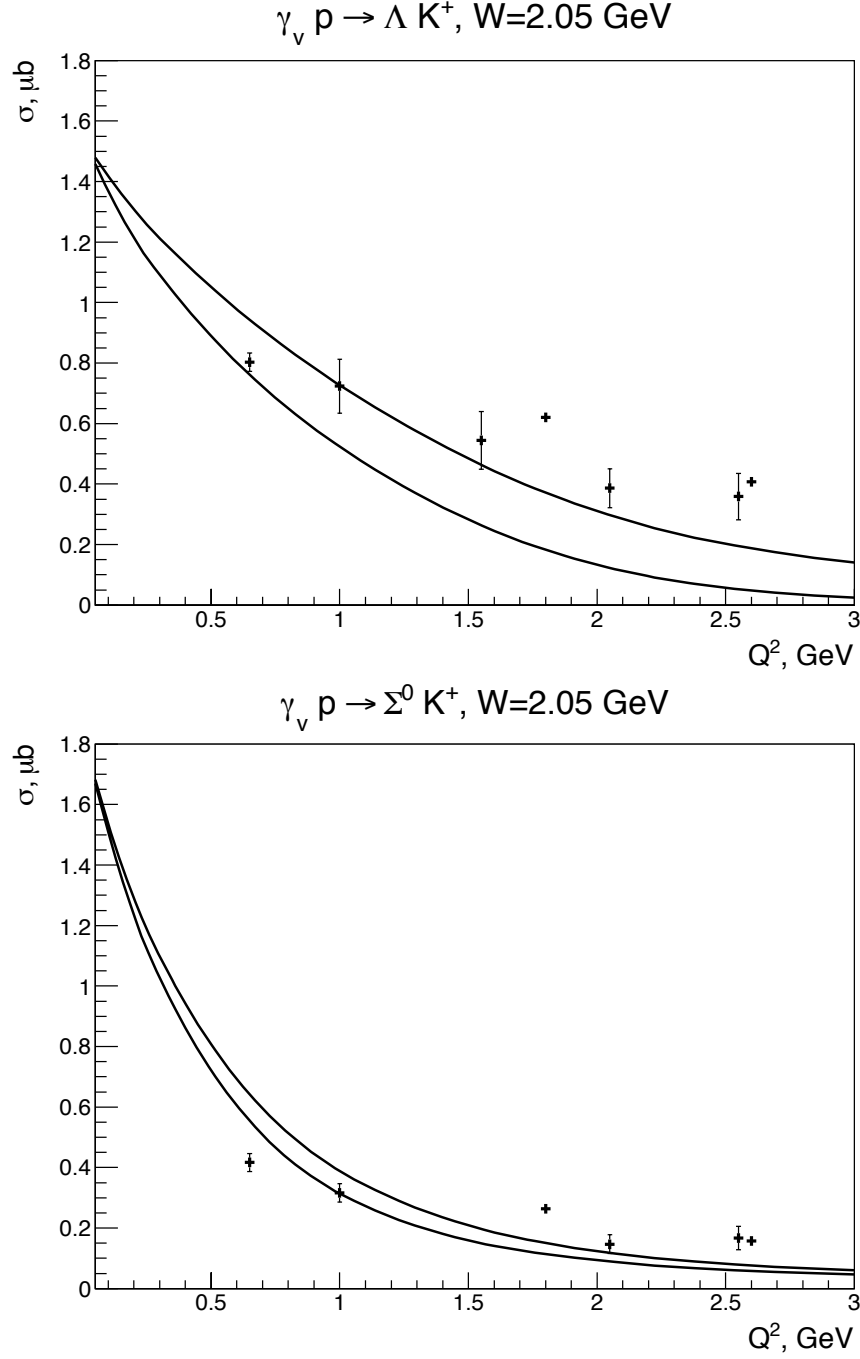


FIG. 14: Integrated cross section for $K^+\Lambda$ (top) and $K^+\Sigma$ (bottom) as a function of Q^2 at $W = 2.05 \text{ GeV}$. Experimental cross sections at $Q^2 = 0.65 \text{ GeV}^2$ are measured at a beam energy of 2.567 GeV . Whereas cross sections at $Q^2 = 1.8 \text{ GeV}^2$ and 2.6 GeV^2 are measured at a beam energy of 5.5 GeV . All other Q^2 points correspond to a beam energy of 4.056 GeV . Model calculations are shown in two curves: upper curve is for a beam energy of 2.567 GeV and lower for 5.5 GeV .

the acceptance is depleted due to the partially blind transition region between the forward and central detectors.

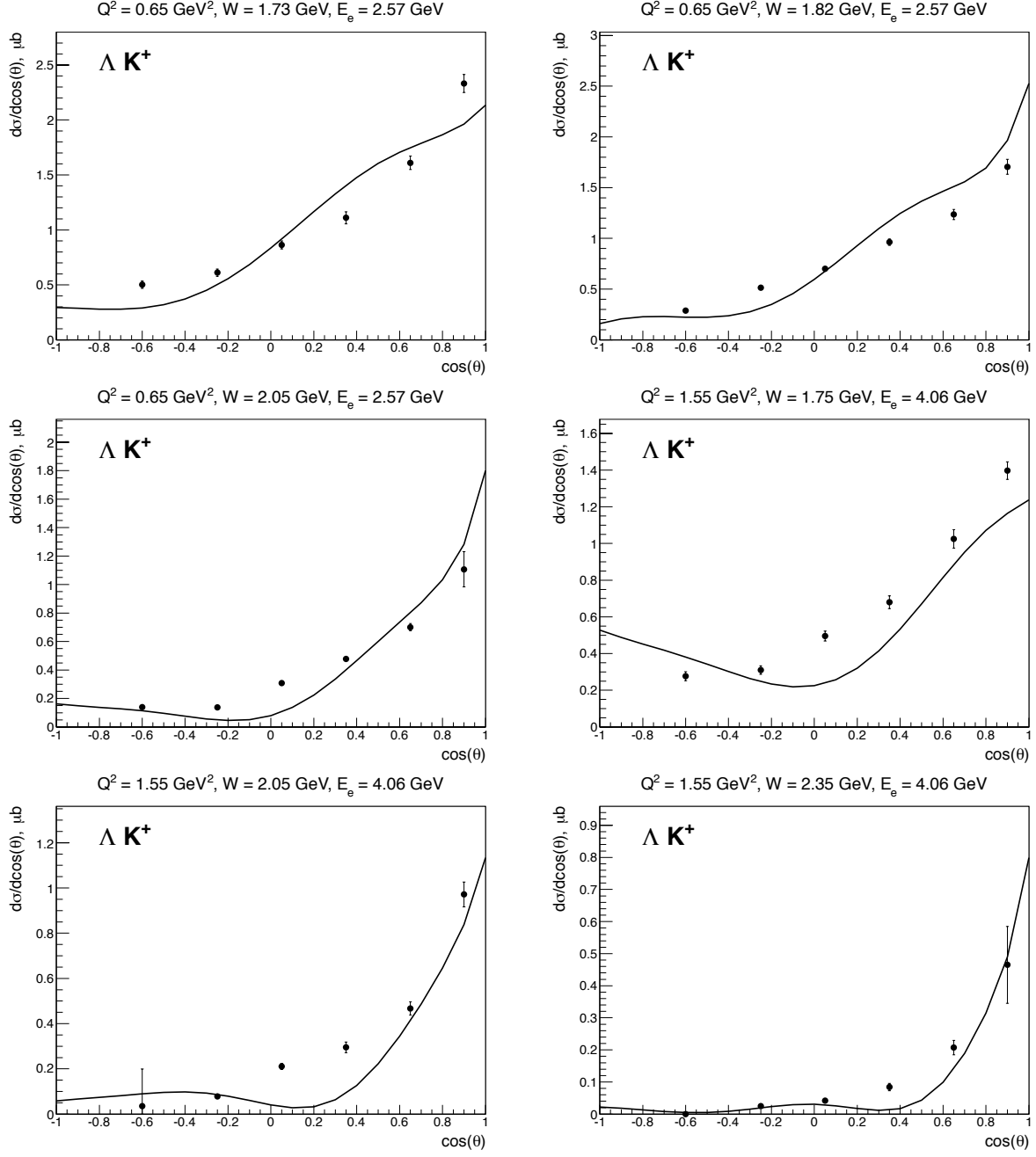


FIG. 15: Differential cross sections for $K^+\Lambda$ channel in certain Q^2 , W bins for two different beam energies. θ is the polar angle of the kaon in the CMS.

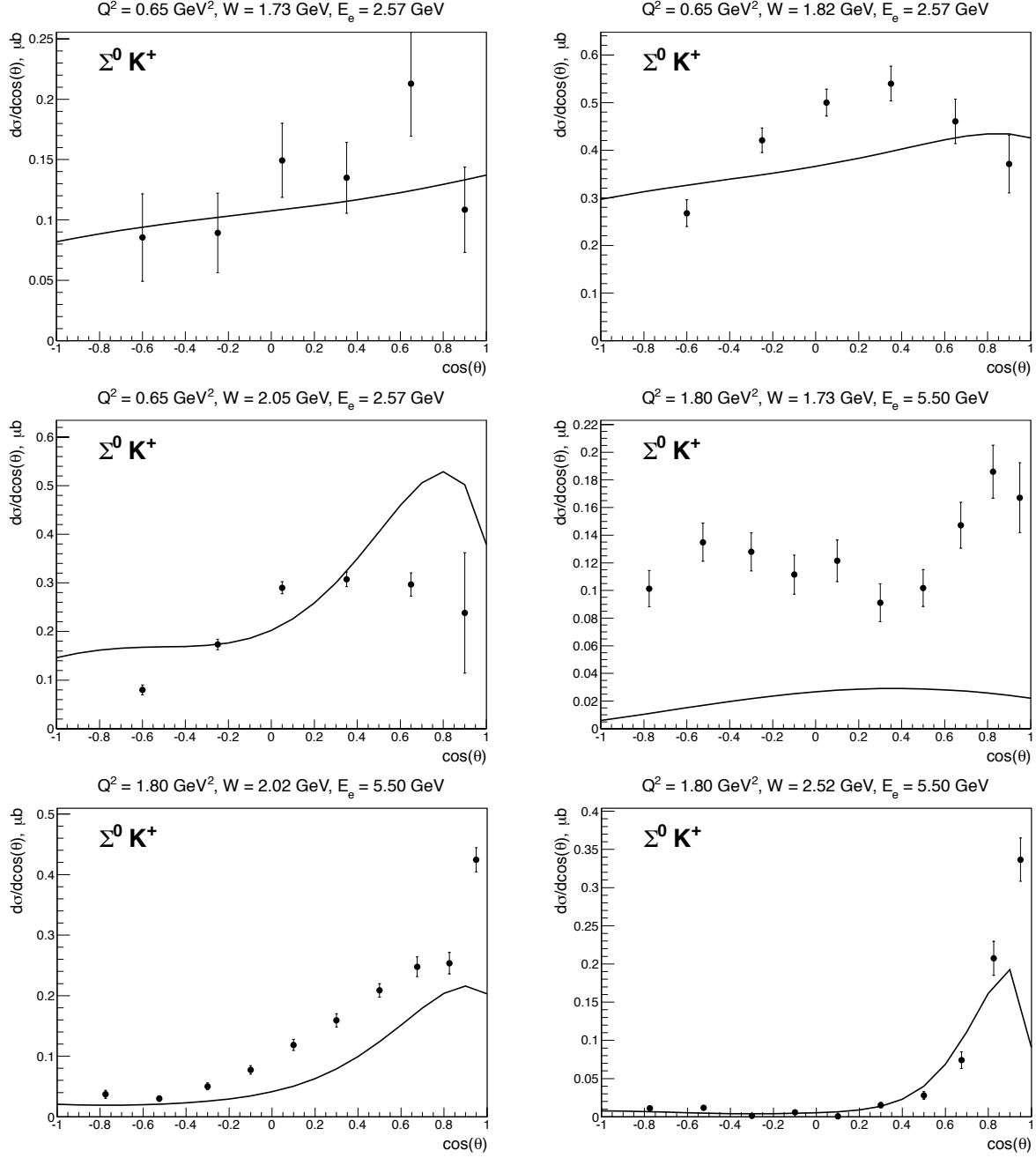


FIG. 16: Differential cross sections for for $K^+\Sigma^0$ channel in certain bins of Q^2 , W bins for some beam energies. θ is polar angle of the kaon in CMS.

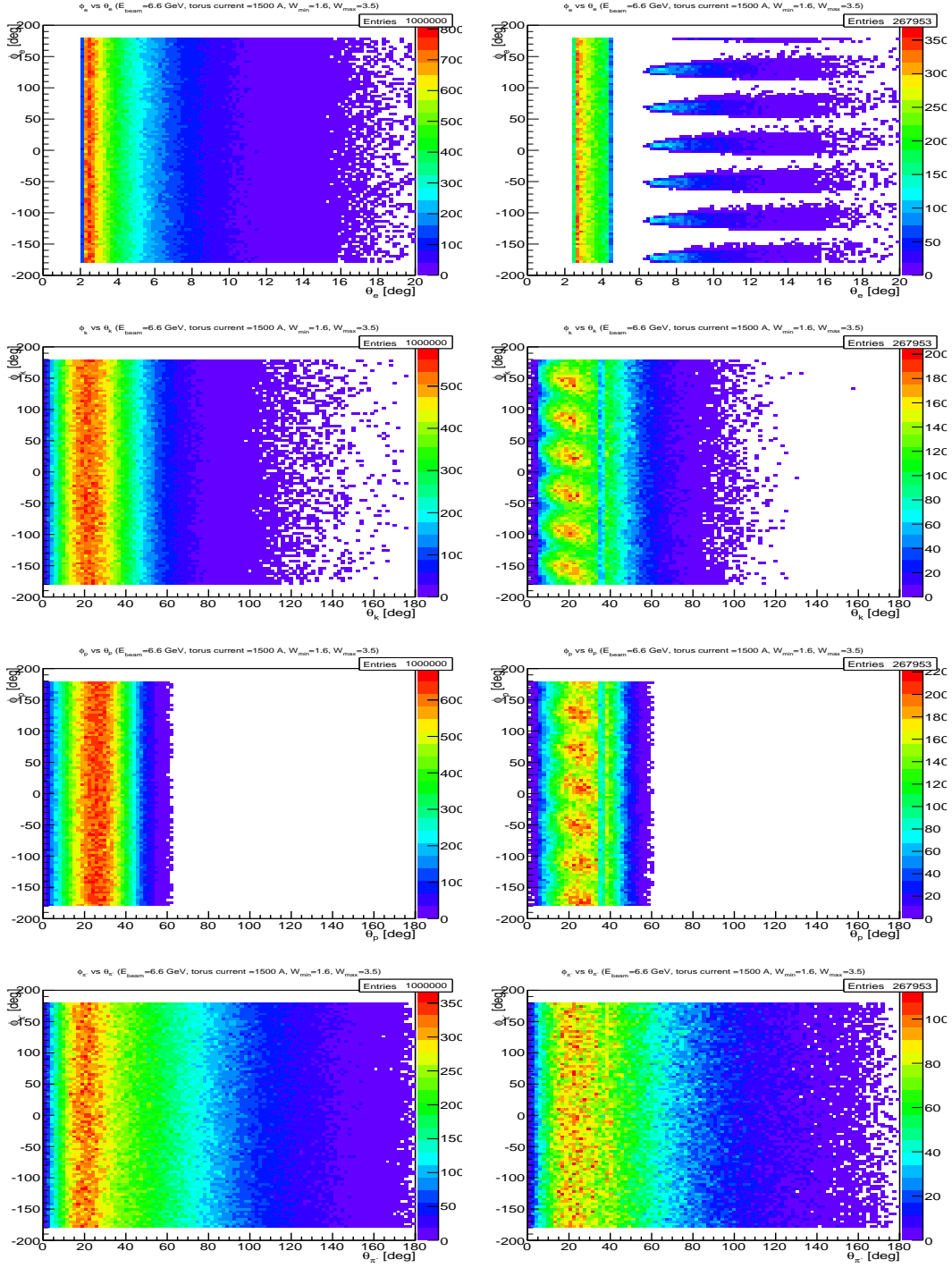


FIG. 17: Azimuthal versus polar angle of generated (left) and accepted events (right) for electrons (top row), K^+ (2nd row), protons (third row), and π^- (bottom row). Events are generated for an electron beam energy of 6.6 GeV in a W range from 1.6 to 3.5 GeV. The torus current is set $I=+1500A$, that bends negatively charged particles inward towards the beamline and reduces the acceptance for electrons within CLAS12.

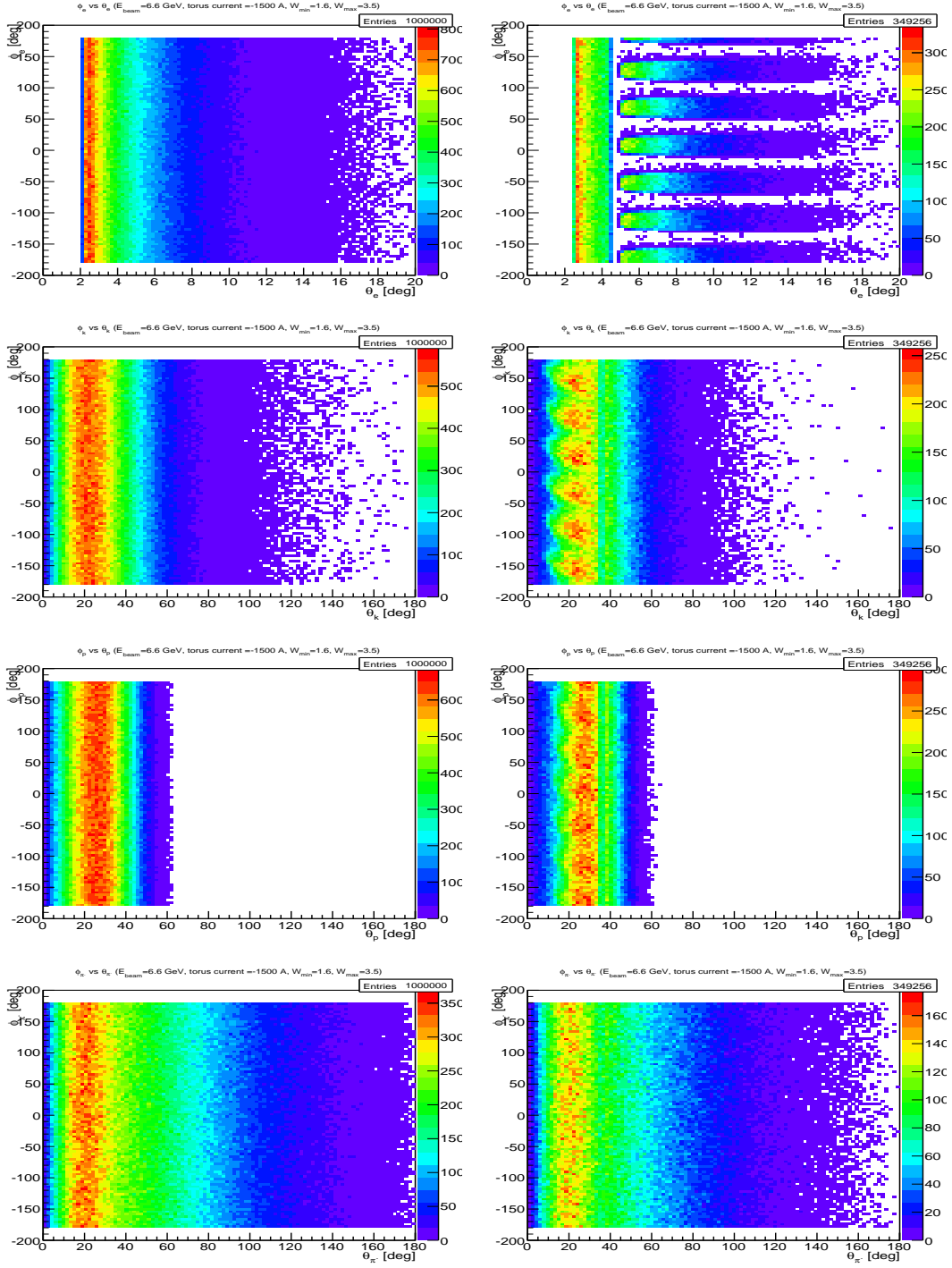


FIG. 18: Azimuthal versus polar angle of generated (left) and accepted events (right) for electrons (top row), K^+ (2nd row), protons (third row), and π^- (bottom row). Events are generated for an electron beam energy of 6.6 GeV in a W range from 1.6 to 3.5 GeV. The torus current is set at $I=-1500$ A, that causes negatively charged particles to bend outwards.

G. Count rates from $K^+\Lambda$

The expected total number of KY electroproduction events in the reaction $ep \rightarrow eK^+Y$ can be written as:

$$N = L \cdot t \cdot \int \frac{d^5\sigma}{dE_e d\Omega_e d\Omega_K^*} dE_e d\Omega_e d\Omega_K^*, \quad (1)$$

where

- $L = 1 \times 10^{35} \text{ cm}^{-2}\text{s}^{-1}$ is expected CLAS12 operating luminosity
- t is expected run time, and
- $\frac{d^5\sigma}{dE_e d\Omega_e d\Omega_K^*}$ is the cross section from (15).

Integration in (1) is performed over the whole kinematic space. The event rate R is defined as $\frac{N}{t}$.

Integration in (1) can be done numerically. We use the same model cross sections for $d^2\sigma/d\Omega_K^*$ as was used in the event generator (see section IV E). The minimum achievable value of Q^2 in CLAS12 is determined by the forward hole, where high energy electrons cannot be detected. For all beam energies Q^2 is greater than 0.01 GeV^2 , so we can integrate in (1) given that $Q^2 > 0.01 \text{ GeV}^2$. The calculated event rates R_Λ and R_{Σ^0} are presented in Table II.

TABLE II: Estimated production rates for events with $Q^2 > 0.01 \text{ GeV}^2$.

$E_{beam}, \text{ GeV}$	$R_\Lambda, \text{ Hz}$	$R_{\Sigma^0}, \text{ Hz}$
6.6	1500	1200
8.8	1400	1100
11	1300	900

To account for the acceptance of CLAS12 a detailed simulation is needed. As we need to generate events in the whole kinematic space with $Q^2 > 0.01 \text{ GeV}^2$, the ratio of reconstructed to generated events gives the averaged acceptance. Multiplying the event rates from Table II by that ratio gives us event rates which account for the acceptance.

An $ep \rightarrow e'K^+\Lambda \rightarrow e'K^+p\pi^-$ event is considered to be reconstructed, if the electron and at least two hadrons have been detected. A trigger condition requiring at least two charged hadrons and an electron would select our channels of interest. Production rate calculations are presented in Table III for all possible beam energies and torus currents. Currently FASTMC is used to estimate the acceptance. A full simulation and reconstruction will be carried out in the near future.

TABLE III: Estimated and acceptance reduced event rates for the channel $ep \rightarrow eK^+\Lambda \rightarrow eK^+p\pi^-$. Electron and two hadrons are required to be accepted.

$E_{beam}, \text{ GeV}$	Torr. cur, A	$R_\Lambda, \text{ Hz}$
6.6	+1500	225
6.6	-1500	240
6.6	+2950	135
6.6	-2950	112
8.8	+1500	168
8.8	-1500	168
8.8	+2950	105
8.8	-2950	82
11	+1500	108
11	-1500	124
11	+2950	100
11	-2950	62

A rough estimate suggests that the KY exclusive channel contribution is about 1% with respect to the two and three pion production, which are expected to dominate the statistics of events that have an electron and at least two charged hadrons in the final state. The total event rate is therefore expected to be $240 \times 100 = 24 \text{ kHz}$ for the trigger condition described above.

H. Expected event rates

At the very forward electron scattering angles, electron rates will be very high and may exceed the capabilities of the data acquisition system. Therefore additional constraints are needed to define an optimal trigger configuration, which would enrich the sample with final state topologies as one might expect them from hybrid baryon candidates and reduce the total acquisition rate. For an initial program we therefore consider to trigger on hadronic final states with at least two charged particles. This will cover final states: $K^+\Lambda \rightarrow K^+p\pi^-$, $p\pi^+\pi^-$, $p\phi \rightarrow pK^+K^-$, $p\eta' \rightarrow p\pi^+\pi^-\eta$. For realistic rate estimates, projections of hadronic coupling strengths of hybrid baryons are needed, which are currently not available. In addition, a single charged hadron trigger will be incorporated with a pre-scaling factor for the FT that will in parallel collect events with a single charged hadron in the final state, i.e. π^+n , $p\pi^0$, $K^+\Lambda$, and $K^+\Lambda$, among others.

The operating luminosity of CLAS12 is estimated at $L = 10^{35} \text{ cm}^2\text{sec}^{-1}$. This corresponds to an event rate of 240 Hz (for $K^+\Lambda$) and about 170 Hz (for $K^+\Sigma^0$). For a 60 day run at that luminosity, the total number of $K^+\Lambda$ events is estimated at 1.2×10^9 , and the number of $K^+\Sigma^0$ events at 0.85×10^9 . The number of events in any histogram for certain smaller intervals of Q^2 and W can be found in the same way. The lowest event rate is expected for high Q^2 and high W . For the kinematics with lowest statistics, e.g. $2.0 \leq Q^2 \leq 2.5 \text{ GeV}^2$ and $2.675 \leq W \leq 2.700 \text{ GeV}$, a total number of 2.0×10^5 $K^+\Lambda$ events and 1.1×10^5 $K^+\Sigma^0$ events are expected.

While these rates seem very large, it should be kept in mind that the signals of hybrid baryons that we want to detect and quantify may be one or two orders of magnitude smaller than the signal from ordinary baryon states and will likely not simply be seen as a peak in the excitation spectrum, but rather as a broad region in W where specific quantum numbers, i.e. $I = \frac{1}{2}$ and $J^P = \frac{1}{2}^+$ or $J^P = \frac{3}{2}^+$, must be identified and the electromagnetic couplings must be measured versus Q^2 . This can be achieved in a partial-wave analysis that includes other channels in a multichannel fit, such as the Bonn-Gatchina or Jülich/GWU approaches. Other techniques may also be employed. Very high statistics is thus essential, and the transverse and longitudinal photon polarization that is inherent in electron scattering will provide amplitude interference and enhance the resonant signal.

V. DATA ANALYSIS

A. Event selection

Electrons will be detected both in the Forward Tagger and in the CLAS12 Forward Detector (FD). Electrons measured in the FD can be identified at scattering angles above 6° in the High-Threshold Cherenkov counter (HTCC) and in the PCAL and EC calorimeters. Due to the higher Q^2 for electrons detected at larger scattering angles in CLAS12 compared to the FT region, the FD electron rate is comparatively much lower than the hadronic rate, which ensures good electron identification.

For electrons detected in the FT, the low Q^2 leads to a very high electron rate that completely dominates the event rate in the FT calorimeter and hodoscope. A direct electron identification at the trigger level is therefore not needed. However the complete event pattern may be checked for consistency with that hypothesis in the event reconstruction. Note that the full electron kinematics is measured in the FT calorimeter and the micromegas tracker and charged particle ID is provided by the two layer hodoscope in front of the calorimeter as well as with hits in the micromegas tracker.

Charged hadrons (π^\pm , K^\pm , and protons) will be tracked in the drift chambers and micromegas in the FD, and in the silicon tracker and barrel micromegas at large angles in the CD. At all angles, charged particle identification is provided in the CLAS12 time-of-flight detector systems. Photons and neutrons are detected at forward angles in the electromagnetic calorimeters (PCAL, EC, FT) and neutrons at large angles are detected in the Central Neutron Detector (CDN).

B. Event reconstruction

The event reconstruction software has been designed and developed to be deployed within the ClaRA framework, a Service Oriented Architecture framework for data processing. The reconstruction application consists of a chain of services which can be deployed within ClaRA. The services for each detector component are compiled as java archive (JAR) plugins which are included in the complete CLAS12 Software release package coatjava. The CLAS12 reconstruction software reconstructs, on an event-by-event basis, the raw data coming from either simulation or the detectors to provide physics analysis output such as track parameters and particle identification. The package

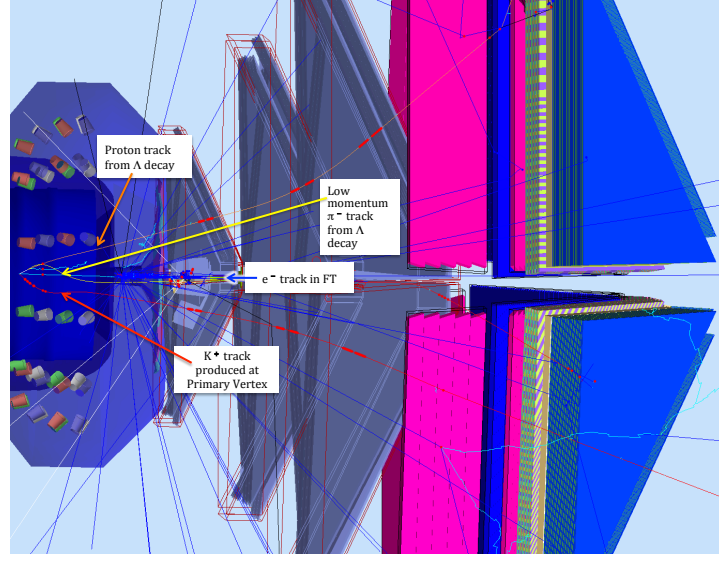
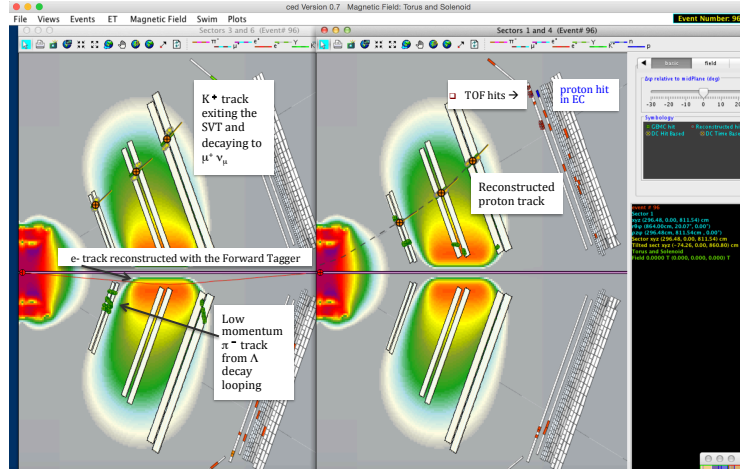


FIG. 19: GEMC - Graphical User Interface Display of $ep \rightarrow e'K^+\Lambda$ ($\Lambda \rightarrow p\pi^-$) event as seen in CLAS12 detectors.



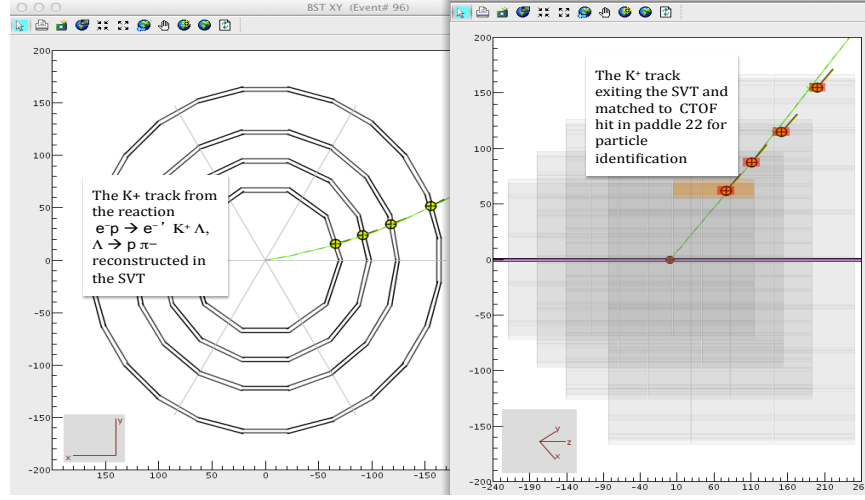
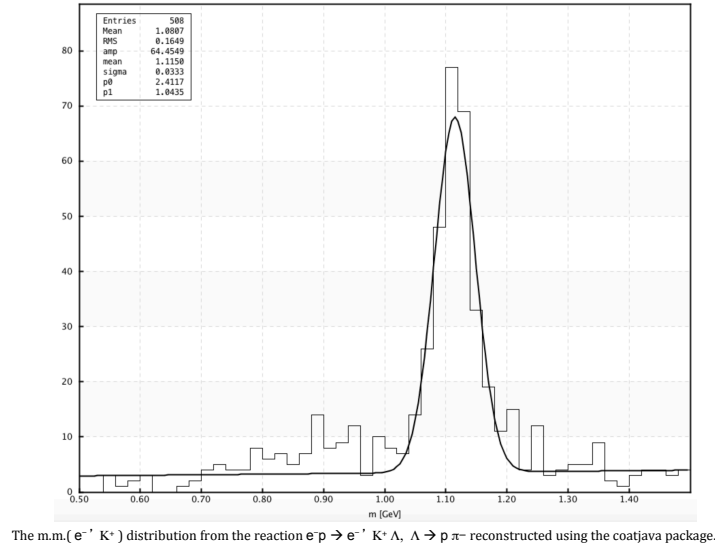
The e- and proton tracks from the reaction $ep \rightarrow e'K^+\Lambda$, $\Lambda \rightarrow p\pi^-$ reconstructed in the Forward Detectors

- The filled orange circles correspond to reconstructed 3-D points obtained from pattern recognition; the tangent to the reconstructed track at the 3-D point is represented by the line segment connected to the filled circle.
- The dashed line corresponds to tracks swam to $z = 0$ with the parameters extracted from the reconstruction algorithm

FIG. 20: Event display for the reaction $ep \rightarrow e'K^+\Lambda$.

provides scripts that can be launched on the farm to cook the data as well as a framework to do event analysis using the flexible scripting language Groovy. The documentation for the coatjava package can be available on the CLAS12 webpage: <http://clasweb.jlab.org/clas12offline/docs/software/html/>. For acceptance and efficiency studies, events are generated using the Geant-4 Monte Carlo simulation application GEMC. A detailed documentation of the detectors included in the simulation and of the various settings used to set the simulation parameters according to physics, backgrounds and magnetic field configurations is available from the gemc webpage: <https://gemc.jlab.org/gemc/Documentation/Documentation.html>. An example of a simulated event for the reaction $ep \rightarrow e'K\Lambda$ is shown in Fig. 19.

At present, the reconstruction software is still in development. The components that are available are the Silicon Vertex Tracker (SVT), the Central Time of Flight (CTOF), the High Threshold Cherenkov Counter (HTCC), the Drift Chambers (DC), the Forward Time-Of-Flight (FTOF), the Electromagnetic and Pre-shower Calorimeters

FIG. 21: Event display for the reaction $ep \rightarrow e' K^+ \Lambda$.The m.m. ($e' K^+$) distribution from the reaction $ep \rightarrow e' K^+ \Lambda$, $\Lambda \rightarrow p \pi^-$ reconstructed using the coatjava package.FIG. 22: Reconstructed Λ mass distribution obtained from the recoil mass against the e' and K^+ for the reaction $ep \rightarrow e' K^+ \Lambda$ at a beam energy of 6.6 GeV. This figure is obtained using the coatjava plotting package (under development).

(EC/PCAL), and the Forward Tagger Calorimeter and Hodoscope. A preliminary version for the Forward MicroMegas Tracker reconstruction is also available and is used to refit the track parameters coming from the DC.

An example of an event for the reaction $ep \rightarrow e' K^+ \Lambda$ run through the reconstruction and displayed using the CLAS12 event display CED is shown in Figs. 20 and 21. An overall Event Builder takes the track momentum and flight path information obtained from Central and Forward tracking and links the track to the outer detector to obtain the responses and determine the PID. The electron is mostly identified by the Forward Tagger for the kinematics of the Hybrid Baryon proposal.

The studies for this letter of intent were done using FastMC. For the proposal these studies will be repeated by generating events with the event generators described in section IV, tracking all particles through CLAS12 with GEMC and subsequently reconstructing these events with coatjava and obtaining the analysis selection criteria using the kinematic fitter available with the package.

An example of a reconstructed Λ mass spectrum obtained from the missing mass against the eK^+ in the reaction $ep \rightarrow e' K^+ \Lambda$ generated with GEMC is shown in Fig. 22. The reconstruction uses only the electron detected in the

Forward Tagger calorimeter and the produced K^+ . Improved mass resolution is obtained when the Λ is reconstructed from the invariant mass of the proton and the π^- .

C. Extracting differential cross sections and normalized yields

After the raw data have been subjected to the CLAS12 event reconstruction software package CLARA, we intend to extract differential cross section for all processes with two-body final states, e.g. KY , $N\pi$, $p\eta$, $p\eta'$, and $p\phi$ using simulations of large amounts of Monte Carlo events to fully understand the acceptances for these processes at the accuracy level required for the partial wave analysis. As for all electroproduction data, the raw cross sections will be subjected to radiative corrections in order to extract the fully corrected differential cross sections. The radiative correction procedure for exclusive processes is well established, and it has been used for correcting single π^+n and $p\pi^0$ production as well as $K^+\Lambda$ and $K^+\Sigma$ electroproduction employing the exact procedure developed in Ref. [19]. As it has been recently demonstrated [20], radiative corrections are very important for the analysis of exclusive processes in terms of resonance excitations as they affect both the polar and azimuthal angular dependencies, and consequently the partial wave analyses based on these processes.

For three-body final states, such as $p\pi^+\pi^-$ and $p\eta\pi^0$, in addition to extracting differential and integrated cross section, we also consider event-based analysis techniques, where acceptances will be assigned to each event, and acceptance weighted events will be subjected to a maximum-likelihood fitting procedure. This procedure preserves the full correlations among the final state particles.

D. Partial wave analysis

Using modern partial wave analysis tools several new excited N^* and Δ^* states have been identified or have been significantly improved in their evidence and their star rating in the 2014 edition of the Review of Particle Properties (RPP) of the Particle Data Group [1]. The use of high statistics photoproduction data from CLAS of a number of final states, e.g. $K^+\Lambda$, $K^+\Sigma$, π^+n , $p\pi^0$, including polarization observables, was essential in establishing this new evidence. This success has also shown the importance of high statistics data sets in the search for new excited states, and has helped to re-vitalize the field of hadron spectroscopy. In the analysis of the data to be taken with the program discussed in this letter-of-intent, we will make full use of these advanced tools of amplitude and partial wave analysis. Significant progress has also been made in the analysis of electroproduction data where transition form factors have been extracted from several excited states using the high statistics data from CLAS [4, 5, 20]. We expect that these data analysis packages will be well-honed by the time the proposed data will be taken, including the extension of the photoproduction analysis to include the existing and planned electroproduction data sets.

E. Strategies for identifying Hybrid Baryons

In this section we address the question if and how gluonic hybrid baryons are distinct from ordinary quark excitations. As discussed in section II B the lowest hybrid baryons should have isospin $I = \frac{1}{2}$ and $J^P = \frac{1}{2}^+$ or $J^P = \frac{3}{2}^+$, and their masses should be in the range of 2.20 to 2.50 GeV. This mass range must be verified once LQCD calculations with physical pion masses become available, as masses may shift with more realistic pion masses, likely to the lower mass range. Four states with $I = \frac{1}{2}$ and $J^P = \frac{1}{2}^+$ are predicted with dominant quark contributions and with masses below the mass of the lowest LQCD hybrid states. Of these four states two are the well known $N(1440)\frac{1}{2}^+$ and $N(1710)\frac{1}{2}^+$, and two are the less well established $N(1880)\frac{1}{2}^+$ and $N(2100)\frac{1}{2}^+$ with 2* and 1* ratings, respectively. Another state $N(2300)$ has a 2* rating, and falls right into the lowest hybrid mass band projected by LQCD. This state, if confirmed, could be a candidate for the predicted lowest LQCD hybrid state.

In order to address this question, it is necessary to confirm (or refute) the existence of the 2* state $N(1880)$ and of the 1* state $N(2100)$, and to measure the electromagnetic couplings of $N(2300)$ and their Q^2 dependence. Improved information on the lower mass states should become available in the next one or two years when the new high-statistics single- and double-polarization data from CLAS have been included into the multi-channel analysis frameworks such as the Bonn-Gatchina or Jülich/GWU approaches. Should these two states be confirmed, then any new nucleon state with $J^P = \frac{1}{2}^+$, which happens to be in the right mass range, could be a candidate for the lowest mass hybrid baryon. The $N(2300)\frac{1}{2}^+$ state has been seen at BES III only in the invariant mass $M(p\pi^0)$ of $\Psi(2S) \rightarrow p\bar{p}\pi^0$ events. In this case the production of $N(2300)$ occurs at very short distances as it emerges from heavy quark flavor $c\bar{c}$ decay.

Hence the state may even be observable in single pion electroproduction $ep \rightarrow e'\pi^+n$ and $ep \rightarrow e'p'\pi^0$, if it couples to photons with sufficient strength to be measurable.

In the $J^P = \frac{3}{2}^+$ sector the situation is more involved. There are two hybrid states predicted in the mass range 2.2 to 2.4 GeV, with masses above five quark model states at same J^P . Of the five states, two are well known 4^* and 3^* states, the $N(1720)\frac{3}{2}^+$ and the $N(1900)\frac{3}{2}^+$, respectively, and one state, the $N(2040)\frac{3}{2}^+$, has a 1^* rating. Here we will have to confirm (or refute) the 1^* star state and find two or three (if $N(2040)$ does not exist) more quark model state with the same quantum numbers in the mass range 1.7 to 2.1 GeV. There is one candidate $\frac{3}{2}^+$ state with mass near 1.72 GeV seen in $p\pi^+\pi^-$ electroproduction [25], whose status we will be able to pin down with the expected very high statistics data.

Possible signatures of the lowest mass hybrid baryons are:

- Resonance masses in the range $2.0 \text{ GeV} \leq W \leq 2.5 \text{ GeV}$ with $I = 1/2$, and $J^P = \frac{1}{2}^+$ or $J^P = \frac{3}{2}^+$
- Q^2 dependence of the transverse helicity amplitude $A_{1/2}(Q^2)$ similar to the $\Delta(1232)\frac{3}{2}^+$ but dissimilar to radially excited states of same J^P , and
- a strongly suppressed helicity amplitude $S_{1/2}(Q^2) \approx 0$ in comparison to other ordinary 3-quark states or meson-baryon excitations.

This list of expected resonance properties may provide some initial guidance when examining new baryon states for signatures of large gluonic components, they are however not sufficient to firmly establish the hybrid nature of a state. To achieve this goal, improved modeling of other degrees-of-freedom such as meson-baryon contributions and direct calculations of electrocouplings from LQCD will be needed. The expected high statistics data will be used to identify any new or poorly known state, whether or not it is a candidate for a hybrid baryon state. This will aid in the identification of the effective degrees of freedom underlying the resonance excitation of all states that couple to virtual photons.

VI. OTHER TOPICS IN LIGHT-QUARK BARYON SPECTROSCOPY THAT ARE ADDRESSED WITH THIS LOI

Besides the search for hybrid baryon states, there are many open issues in our knowledge of the structure of ordinary baryon excitations, that can be addressed with data taken in parallel from the same experiment. As an example we show in Fig. 23 the electrocouplings of the $N(1680)\frac{5}{2}^+$ resonance, the strongest state in the third nucleon resonance region. With the exception of the real photon point, the data are quite sparse for $Q^2 \leq 1.8 \text{ GeV}^2$ and the high statistics data expected from this project would remedy the lack of experimental information and address similar situations for other states as well. Note that the very high Q^2 part will be covered by the approved JLab experiment E12-09-003.

An even more compelling example is the $N(1675)\frac{5}{2}^-$ state, where data at $Q^2 > 1.8 \text{ GeV}^2$ have been published recently by the CLAS Collaboration [20]. Figure 24 shows the measured helicity amplitudes. Low Q^2 data are very important here, as for this state the quark transitions are strongly suppressed by the Moorhouse selection rule, and therefore, any non-zero value of the electrocoupling amplitudes will directly measure the strength of the meson-baryon contributions. The main data needed are single pion production $ep \rightarrow e'\pi^+n$ and $ep \rightarrow e'\pi^0p$. These processes can be accumulated with sufficiently high event rates, even with a pre-scale factor of 10 or more on the FT, should the overall event rate be too high in this 2-prong topology.

VII. BEAMTIME ESTIMATE

The complete hybrid baryon program will require 3 beam energies, 6.6 GeV, 8.8 GeV, and 11 GeV, to cover with high statistics the lowest Q^2 range where the scattered electron is detected in the angle range from $2.5^\circ \leq \theta_e \leq 4.5^\circ$. For the proposal we will likely request new beam time of 60 days that are divided into 20 days at 6.6 GeV and 40 days at 8.8 GeV. The 11 GeV data of 60 days can be taken simultaneously with the already approved experiment E12-11-005.

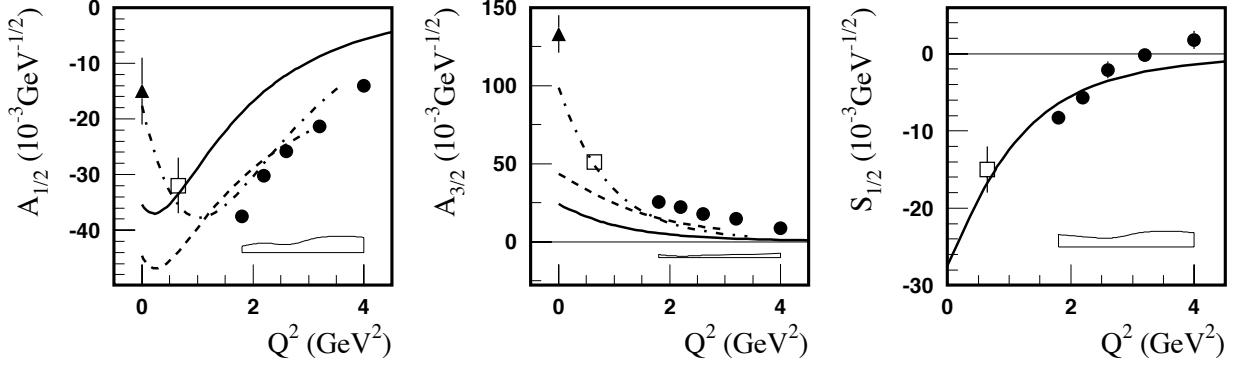


FIG. 23: Electrocoupling amplitudes of the $N(1680)_{\frac{1}{2}}^{5+}$ resonance.

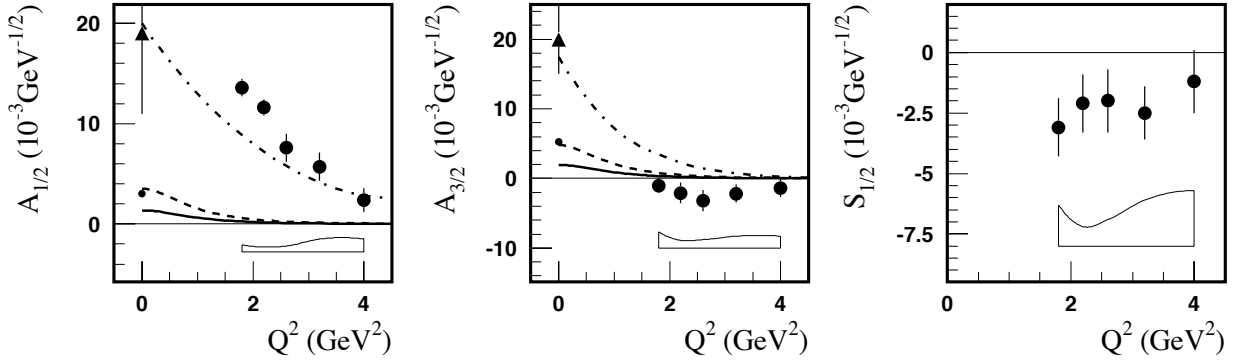


FIG. 24: Electrocoupling amplitudes of the $N(1675)_{\frac{1}{2}}^{5-}$ resonance. Quark models predict the transverse amplitudes to be suppressed. The significant deviation of the $A_{1/2}$ amplitudes is consistent with meson-baryon contributions to the excitation strength (dashed-dotted lines).

VIII. SUMMARY

In this Letter-of-Intent we laid out an extensive program to study the excitation of nucleon resonances in meson electroproduction using electron beam energies of 6.6, 8.8, and 11 GeV. The main focus is on the search for gluonic light-quark baryons in the mass range up to 3.5 GeV and in the Q^2 range from 0.05 to 2.0 GeV^2 . We have estimated the rates for two of the channels we propose to study, $K^+\Lambda$ ($K^+\Sigma$) and $p\pi^+\pi^-$, but all other channels detected in CLAS12 will be subjected to analyses as well. The expected rates are very high, thanks to the very forward scattered electrons with a minimum Q^2 of 0.05 GeV^2 that are detected in the Forward Tagger. The data will be subjected to state-of-the-art partial wave analyses that were developed during the past years for baryon resonance analyses. Beyond the main focus of this LOI on hybrid baryons, a wealth of data will be collected in many different channels that will put meson electroproduction data on par with real photoproduction in terms of production rates and will allow for a vast extension of the ongoing N^* electroexcitation program with CLAS at lower energies. It will complement the already approved program to study nucleon resonance excitations at the highest Q^2 achievable at 11 GeV beam energy.

IX. PLANNED MONTE-CARLO STUDIES FOR HYBRID BARYON MANIFESTATION IN EXCLUSIVE KY ELECTROPRODUCTION

In this section we discuss more details of our current thinking on how to establish the presence of hybrid states in the proposed experiment. The proposed studies will be fleshed out in more detail in the full proposal, that we plan to submit to a future PAC.

The feasibility to observe hybrid baryons will be explored in more detail in a Monte-Carlo simulation of KY electroproduction. The KY polar and azimuthal angle distributions for the final kaon in the center-of-mass (CMS), θ_K and ϕ_K , will be simulated using two reaction models for the KY electroproduction cross sections based on the CLAS12 acceptance:

- the coherent superposition of reggeized non-resonant amplitudes and the contributions from the established N^* states [17, 29], the web-site [30] provides a full set of KY electroproduction observables off proton (model A), and
- incoherently adding to model A hypothetical cross sections for the KY production due to new hybrid baryon state in the virtual-photon-proton s-channel (model B)

Comparing the CMS angle distributions of the final kaons simulated according to models A and B will allow us to determine the minimal absolute values of the hybrid baryon electroexcitation amplitudes that are needed to re-identify them in the analysis of the reconstructed data. We will focus on exploration of feasibility to observe the lightest hybrid baryons of minimal decay widths, that makes the expected signals from such hybrid states the most pronounced.

Lattice QCD [11] predicts, as shown in Fig. 1, two lightest hybrid states of ≈ 2.6 GeV mass with spin-parities $J^P = \frac{1}{2}^+$ and $\frac{3}{2}^+$. Since these Lattice QCD studies were carried out with a pion mass above the physical value, we are correcting the predicted hybrid baryon masses by employing mass shifts for both states towards smaller values, which can be expected when the physical pion mass is reached. The mass shift for the lowest hybrid baryon with $J^P = \frac{1}{2}^+$ spin-parity can be estimated by the difference between the LQCD result [11] for the mass of the lightest nucleon of spin-parity $J^P = \frac{1}{2}^+$ and the measured value of the proton mass, $\Delta_1=0.3$ GeV. For the lowest hybrid state with $J^P = \frac{3}{2}^+$, the mass shift can be estimated by the differences between the mass of the lightest LQCD resonance with $J^P = \frac{3}{2}^+$ and the physical mass of the $N(1720)\frac{3}{2}^+$ four star resonance, $\Delta_2=0.5$ GeV. Therefore, we will implement hybrid baryons with spin-parities $J^P = \frac{1}{2}^+$ and $J^P = \frac{3}{2}^+$ in the mass range from 2.1 to 2.3 GeV into the simulation of the KY cross section by employing model B. According to the RPP14 results [1] on the resonance parameters in the mass range around 2.0 GeV, we adopt for the total decay width of hybrid baryons a range from 250 to 300 MeV and for their branching fraction (BF) to the KY final states the value of 5%.

The cross sections integrated over the angle ϕ_K produced by a hybrid baryon state can be evaluated from the resonant hybrid electroexcitation amplitudes according to (23,25) in the Appendix, replacing the full two-body amplitudes by the resonant contributions from the hybrid resonance. A relativistic Breit-Wigner (BW) ansatz gives the following expression for the $\langle \lambda_f | T_r | \lambda_\gamma \lambda_p \rangle$ resonant amplitude of a single hybrid resonance in the helicity representation:

$$\langle \lambda_f | T_r | \lambda_\gamma \lambda_p \rangle = \frac{\langle \lambda_f | T_{dec} | \lambda_R \rangle \langle \lambda_R | T_{em} | \lambda_\gamma \lambda_p \rangle}{M_r^2 - W^2 - i\Gamma_r M_r}, \quad (2)$$

where M_r and Γ_r are the resonance mass and total width, respectively. For the particular purpose of the cross section evaluation for the event generator we employ the energy independent total/partial resonance decay widths.

The matrix elements $\langle \lambda_R | T_{em} | \lambda_\gamma \lambda_p \rangle$ and $\langle \lambda_f | T_{dec} | \lambda_R \rangle$ are the electromagnetic production and hadronic decay amplitudes of the N^* with helicity $\lambda_R = \lambda_\gamma - \lambda_p$, in which λ_γ and λ_p stand for the helicities of the photon and proton in the initial state, and λ_f represents the helicity of final-state hadron in the N^* decays. The hadronic decay amplitudes $\langle \lambda_f | T_{dec} | \lambda_R \rangle$ are related to the Γ_{λ_f} partial hadronic decay widths of the N^* to KY final states f of helicity $\lambda_f = \lambda_Y$ by:

$$\langle \lambda_f | T_{dec} | \lambda_R \rangle = \langle \lambda_f | T_{dec}^{J_r} | \lambda_R \rangle d_{\mu\nu}^{J_r}(\cos \theta_K) e^{i\mu\phi_K},$$

with $\mu = \lambda_R$ and $\nu = -\lambda_Y$, and

$$\langle \lambda_f | T_{dec}^{J_r} | \lambda_R \rangle = \frac{2\sqrt{2\pi}\sqrt{2J_r+1}M_r\sqrt{\Gamma_{\lambda_f}}}{\sqrt{p_i^r}} \sqrt{\frac{p_i^r}{p_i}}. \quad (3)$$

p_i^r and p_i are the magnitudes of the three-momenta of the final state K for the $N^* \rightarrow K\Lambda$ decay ($i=1$) or for the $N^* \rightarrow K\Sigma$ decay ($i=2$), evaluated at $W = M_r$ and at the running W , respectively. The variables θ_K , ϕ_K are the CMS polar and azimuthal angles for the final kaon, and J_r stands for the N^* spin.

The final state Λ or Σ baryons can only be in the helicity states $\lambda_f = \pm\frac{1}{2}$. The hadronic decay amplitudes $\langle\lambda_f|T_{dec}^{J_r}|\lambda_R\rangle$ with $\lambda_f = \pm\frac{1}{2}$ are related by P-invariance, which imposes the absolute values for both amplitudes to be the same. Therefore, the hybrid state partial decay widths to the $K\Lambda$ and $K\Sigma$ final states Γ_{λ_f} can be estimated as:

$$\Gamma_{\lambda_f} = \frac{1}{2}\Gamma_r 0.05, \quad (4)$$

where the factor 0.05 reflects the adopted 5% BF for hybrid baryon decays to the KY final state.

The following relationships between the transition amplitudes $\langle\lambda_R|T_{em}|\lambda_\gamma\lambda_p\rangle$ and the $\gamma_v NN^*$ electrocouplings were obtained in the paper [26]:

$$\begin{aligned} \langle\lambda_R|T_{em}|\lambda_\gamma\lambda_p\rangle &= \frac{W}{M_r} \sqrt{\frac{8M_N M_r q_{\gamma r}}{4\pi\alpha}} \sqrt{\frac{q_{\gamma r}}{q_\gamma}} A_{1/2,3/2}(Q^2), \\ \text{with } |\lambda_\gamma - \lambda_p| &= \frac{1}{2}, \frac{3}{2} \text{ for transverse photons, and} \\ \langle\lambda_R|T_{em}|\lambda_\gamma\lambda_p\rangle &= \frac{W}{M_r} \sqrt{\frac{16M_N M_r q_{\gamma r}}{4\pi\alpha}} \sqrt{\frac{q_{\gamma r}}{q_\gamma}} S_{1/2}(Q^2), \\ &\text{for longitudinal photons,} \end{aligned} \quad (5)$$

where q_γ is the absolute value of the initial photon three-momentum of virtuality $Q^2 > 0$ with $q_\gamma = \sqrt{Q^2 + E_\gamma^2}$ and E_γ the photon energy in the CMS frame at the running W

$$E_\gamma = \frac{W^2 - Q^2 - M_N^2}{2W}. \quad (6)$$

The $q_{\gamma,r}$ value is then computed from (6) with $W=M_r$.

Inserting the production amplitudes (2), (3), and (5) for a single resonance, which in this case is a hybrid baryon candidate, into the currents determined by (25), leads to the final expressions for the transverse $\frac{d\sigma_{TH}}{d(-\cos(\theta_K))}$ and the longitudinal $\frac{d\sigma_{LH}}{d(-\cos(\theta_K))}$ ϕ_K integrated single-differential cross section for KY electroproduction off unpolarized protons for the hybrid state electroexcitation from (23) with density matrices for the initial and the final states determined by (18) :

$$\begin{aligned} \frac{d\sigma_{TH}}{d(-\cos(\theta_K))} &= \frac{4\pi\alpha}{4K_L M_N} \frac{1}{2} \frac{1}{2} \sum_{\lambda_\gamma=\pm 1, \lambda_p, \lambda_f} \frac{\langle\lambda_R|T_{em}|\lambda_\gamma\lambda_p\rangle^2 \langle\lambda_f|T_{dec}^{J_r}|\lambda_R\rangle^2 d_{\mu\nu}^{J_r^2}(\cos\theta_K)}{(M_r^2 - W^2)^2 + (\Gamma_r M_r)^2} \frac{q_K}{2\pi 4W}, \\ \frac{d\sigma_{LH}}{d(-\cos(\theta_K))} &= \frac{4\pi\alpha}{4K_L M_N} \frac{1}{2} \sum_{\lambda_\gamma=0, \lambda_p, \lambda_f} \frac{\langle\lambda_R|T_{em}|\lambda_\gamma\lambda_p\rangle^2 \langle\lambda_f|T_{dec}^{J_r}|\lambda_R\rangle^2 d_{\mu\nu}^{J_r^2}(\cos\theta_K)}{(M_r^2 - W^2)^2 + (\Gamma_r M_r)^2} \frac{q_K}{2\pi 4W}, \end{aligned} \quad (7)$$

$$\begin{aligned} \mu &= \lambda_\gamma - \lambda_p, \\ \nu &= -\lambda_Y, \end{aligned}$$

Resonance electroproduction $\langle\lambda_R|T_{em}|\lambda_\gamma\lambda_p\rangle$ and hadronic decay $\langle\lambda_f|T_{dec}^{J_r}|\lambda_R\rangle$ amplitudes are determined by (5) and (3), respectively.

Assuming only contribution from unpolarized structure functions described in the Appendix A by (19,24), the two fold differential cross sections produced by the hybrid resonance $\frac{d\sigma_H}{d\Omega_K}$ can be computed as:

$$\frac{d\sigma_H}{d\Omega_K} = \frac{1}{2\pi} \left[\frac{d\sigma_{TH}}{d(-\cos(\theta_K))} + \epsilon_L \frac{d\sigma_{LH}}{d(-\cos(\theta_K))} \right]. \quad (8)$$

Differential cross sections computed according to (7,8) should be added incoherently to the model [17, 29, 30] differential cross sections in order to obtain differential cross sections for KY electroproduction according to model B, which accounts for the contributions from hybrid baryon state. In both model A and model B they should be converted

to the four-fold measurable electroproduction cross sections employing (12) of Appendix A. These measurable cross sections should be used in the event generator for the simulation of KY events produced in electron scattering off protons with and without hybrid baryon contributions.

The difference in the angular distributions of the reconstructed KY events simulated in the models A and B will tell us whether a given hybrid baryon state can be observed.

In order to quantify the statistical significance of the difference between the exclusive KY event distributions over the θ_K , ϕ_K CMS angles as simulated according to the models A and B, the following $\chi^2/d.p.$ definition will be used:

$$\chi^2/d.p. = \frac{1}{N_{d.p.}} \sum_{\theta_i, \phi_j, W_k} \frac{(N_{B_{i,j,k}} - N_{A_{i,j,k}})^2}{\delta_{i,j,k}^2}, \quad (9)$$

where $N_{A_{i,j,k}}$, $N_{B_{i,j,k}}$ are the numbers of KY events in the kinematic bins of θ_i , ϕ_j and W_k simulated in the models A and B, respectively, taking into account the CLAS12 acceptance, θ_i and ϕ_i stand for the polar and azimuthal emission angles of kaon in the CMS frame, the sum runs over all bins over θ_K , ϕ_K , and W within any given bin of Q^2 . The $N_{d.p.}$ is the total number of θ , ϕ , and W bins that are included in the sum (9). The values of $\chi^2/d.p.$ should be evaluated independently in each Q^2 bin. The θ_K - and ϕ_K CMS angles are running from 0^0 to 180^0 and from 0^0 to 360^0 , respectively. The sum over W ranges from 1.9 GeV to 2.4 GeV, which is predicted to be the most sensitive range for low-lying hybrid baryon contributions. Assuming that the statistical uncertainties dominate, the uncertainties for the differences ($N_{B_{i,j,k}} - N_{A_{i,j,k}}$) between the event distributions simulated in the models B and A, respectively, can be evaluated as:

$$\delta_{i,j,k} = \sqrt{N_{A_{i,j,k}} + N_{B_{i,j,k}}}. \quad (10)$$

We will investigate hybrid baryon states with spin-parities $J^P = \frac{1}{2}^+$ and $\frac{3}{2}^+$. Electroexcitation of the former state can be described by two electrocouplings $A_{1/2}$ and $S_{1/2}$, while the latter should be described by three electrocouplings, $A_{1/2}$, $S_{1/2}$, and $A_{3/2}$. The definitions of all electrocouplings can be found in the review [5]. Information on the expected Q^2 -evolution of the aforementioned electrocouplings for hybrid states is, to the best of our knowledge, currently not available. We will vary the hybrid baryon electrocouplings to determine their minimal absolute values above which the signal from the hybrid baryon can be observed in the difference between the angular distributions with and without hybrid baryon contributions. These studies will be independently done in each Q^2 bin of the proposed experiment.

The following restrictions will be imposed in the variation of the hybrid baryon electrocouplings, assuming positive values of all electrocouplings.

- **the hybrid baryon of $\frac{3}{2}^+$ spin-parity:** Three electrocouplings $A_{1/2}$, $S_{1/2}$, and $A_{3/2}$ will be computed varying the positive parameter A as:

$$\begin{aligned} A_{1/2} &= A, \\ S_{1/2} &= AQ, \\ A_{3/2} &= A/Q^2, \\ Q &= \sqrt{Q^2} \end{aligned} \quad (11)$$

The relations (11) for the hybrid baryon electrocouplings have been used in the modeling [9] of the hybrid baryon signatures.

- **Hybrid baryon with $\frac{1}{2}^+$ spin-parity:** Electrocouplings will be varied under two assumptions: a) $S_{1/2}=0$ $\text{GeV}^{-1/2}$ as predicted by model [15] for the hybrid $N(1440)1/2^+$ resonance, and b) the relations (11) with $A_{3/2}=0$ $\text{GeV}^{-1/2}$ will be employed.

The $\chi^2/d.p.$ values, calculated according to (9) will elucidate the feasibility of hybrid baryon observation. The $\chi^2/d.p.$ values above 2 will be considered as the statistically significant signals for hybrid baryon states. Consequently, the minimal absolute values of hybrid baryon electrocouplings, above which $\chi^2/d.p.$ becomes larger than 2, will be treated as the minimal values of hybrid electrocouplings, above which the signal from a hybrid baryon can be observed in the proposed experiment.

X. APPENDIX A

The exclusive reaction cross sections for photon absorption by the proton $\frac{d^2\sigma}{d\Omega_K}$ can be determined in the single photon exchange approximation based on the conventions for the production amplitudes explained in [31]. These cross sections are related to the measured exclusive electron scattering cross sections $\frac{d^4\sigma}{dWdQ^2d\Omega_K}$ by:

$$\frac{d^4\sigma}{dWdQ^2d\Omega_K} = \Gamma_v \frac{d^2\sigma}{d\Omega_K}, \quad (12)$$

where Γ_v is the virtual photon flux defined by the momenta of the incoming and outgoing electrons:

$$\Gamma_v = \frac{\alpha}{4\pi} \frac{1}{E_b^2 M_p^2} \frac{W(W^2 - M_p^2)}{(1 - \varepsilon)Q^2}, \quad (13)$$

and α is the fine structure constant, E_b is the beam energy, M_p is the proton mass, and ε is the virtual photon transverse polarization given by

$$\varepsilon = \left(1 + 2 \left(1 + \frac{\nu^2}{Q^2} \right) \tan^2 \left(\frac{\theta_e}{2} \right) \right)^{-1}, \quad (14)$$

where ν is the virtual photon energy, θ_e is the electron scattering angle in the laboratory frame, and $d\Omega_K$ the element of the solid angle of kaon emission in the CMS frame.

Alternatively, the exclusive electron scattering cross sections off protons $\frac{d^5\sigma}{dE'd\Omega_{e'}d\Omega_K}$ can be obtained employing another set of variables for the scattered electron, where dE' and $d\Omega_{e'}$ represent the differentials for energy and solid angle of the scattered electron in the lab frame:

$$\begin{aligned} \frac{d^5\sigma}{dE'd\Omega_{e'}d\Omega_K} &= \Gamma'_v \frac{d^2\sigma}{d\Omega_K}, \\ \Gamma'_v &= \frac{\alpha}{2\pi^2} \frac{E_{e'}}{E_b} \frac{(W^2 - M_p^2)}{(1 - \varepsilon)2M_p Q^2}. \end{aligned} \quad (15)$$

The formalism that relates the amplitude for exclusive hadron electroproduction off protons to the measurable cross sections is described in details in [33]. Here we outline the part of this formalism which is relevant to the studies proposed in the LOI. The two-fold differential cross section $\frac{d^2\sigma}{d\Omega_K}$ for KY electroproduction off the protons can be computed as a contraction of leptonic and hadronic tensors divided by the invariant virtual photon flux and multiplied by the phase space differential for the two-body final state $d^2\Phi$:

$$d^2\Phi = \frac{q_K d\Omega_K}{4\pi^2 4W}, \quad (16)$$

where q_K is the absolute value of the kaon three momentum in the CMS frame. The leptonic tensor $L_{\mu\nu}$ is well known from QED [33]. The hadronic tensor $W_{\mu\nu}$ represents a product of the hadronic currents J_μ^* and J_ν contracted with the spin-density matrices for the initial and the final hadrons $\rho_{\lambda_{p'}, \lambda_p}, \rho_{\lambda_{f'}, \lambda_f}$:

$$W_{\mu\nu} = \sum_{\lambda_{p'}, \lambda_p, \lambda_{f'}, \lambda_f} J_\mu^*(\lambda_{p'}, \lambda_{f'}) J_\nu(\lambda_p, \lambda_f) \rho_{\lambda_{p'}, \lambda_p} \rho_{\lambda_{f'}, \lambda_f}, \quad (17)$$

where $\lambda_{p'}$, λ_p , and $\lambda_{f'}$, λ_f stand for the helicities of the initial proton and for the helicities of the final hadrons, respectively. The sum is running over repetitive indices. In a case of an unpolarized initial proton and unpolarized final hadrons, the density matrices can be written as:

$$\begin{aligned} \rho_{\lambda_{p'}, \lambda_p} &= \frac{1}{2} I, \text{ and} \\ \rho_{\lambda_{f'}, \lambda_f} &= I, \end{aligned} \quad (18)$$

where I is the unity matrix.

Contracting the leptonic [33] and hadronic (17) tensors in the lab frame, we obtain the following expression for two-fold differential KY cross section $\frac{d\sigma}{d\Omega_K}$:

$$\begin{aligned} \frac{d\sigma}{d\Omega_K} = & \frac{4\pi\alpha}{4K_L M_N} \left[\frac{J_x^* J_x + J_y^* J_y}{2} + \epsilon_L J_z^* J_z \right. \\ & \left. + \epsilon_T \frac{J_x^* J_x - J_y^* J_y}{2} + \sqrt{2\epsilon_L(1+\epsilon_T)} \frac{J_x^* J_z + J_z^* J_x}{2} \right] \frac{q_K}{4\pi^2 4W}, \end{aligned} \quad (19)$$

where α is fine structure constant and ϵ_L stands for degree of longitudinal polarization of virtual photons. QED gives for ϵ_L [33]:

$$\epsilon_L = \sqrt{\frac{Q^2}{\nu^2}} \epsilon. \quad (20)$$

The factor $4K_L M_N$ is the invariant virtual photon flux with M_N is nucleon mass and K_L is the equivalent photon energy:

$$K_L = \frac{W^2 - M_N^2}{2M_N}. \quad (21)$$

The four terms in (19) generate four structure functions that define the exclusive electroproduction cross section, transverse (T), longitudinal (L), and two interference structure functions transverse-transverse (TT) and transverse-longitudinal (TL):

$$\frac{d\sigma}{d\Omega_K} = \frac{d\sigma_T}{d\Omega_K} + \epsilon_L \frac{d\sigma_L}{d\Omega_K} + \epsilon_T \frac{d\sigma_{TT}}{d\Omega_K} \cos(2\phi_K) + \sqrt{2\epsilon_L(1+\epsilon_T)} \frac{d\sigma_{TL}}{d\Omega_K} \cos(\phi_K). \quad (22)$$

After integration of the two-fold differential cross section (19, 22) $d^2\sigma/d\Omega_K$ over the azimuthal ϕ_K angle of the final K , all interference structure functions disappear and the (19, 22) are reduced to the simpler expressions:

$$\frac{d\sigma}{d(-\cos(\theta_K))} = \frac{4\pi\alpha}{4K_L M_N} \left\{ \frac{J_x^* J_x + J_y^* J_y}{2} + \epsilon_L J_z^* J_z \right\} \frac{q_K}{2\pi 4W}, \quad (23)$$

and

$$\frac{d\sigma}{d(-\cos(\theta_K))} = \frac{d\sigma_T}{d(-\cos(\theta_K))} + \epsilon_L \frac{d\sigma_L}{d(-\cos(\theta_K))}. \quad (24)$$

The hadronic current J_ν in the lab frame is related to reaction helicity amplitudes [31]:

$$\begin{aligned} J_x &= -\frac{\langle \lambda_f | T | \lambda_p \lambda_\gamma = 1 \rangle - \langle \lambda_f | T | \lambda_p \lambda_\gamma = -1 \rangle}{\sqrt{2}}, \\ J_y &= i \frac{\langle \lambda_f | T | \lambda_p \lambda_\gamma = 1 \rangle + \langle \lambda_f | T | \lambda_p \lambda_\gamma = -1 \rangle}{\sqrt{2}}, \text{ and} \\ J_z &= \frac{\nu}{\sqrt{Q^2}} \langle \lambda_f | T | \lambda_p \lambda_\gamma = 0 \rangle. \end{aligned} \quad (25)$$

The J_0 component of the hadronic current is determined by the current conservation:

$$q_0 J^0 - q_z J^z = 0. \quad (26)$$

-
- [1] K. A. Olive *et al.* [Particle Data Group Collaboration], Chin. Phys. C **38**, 090001 (2014)
 - [2] I. G. Aznauryan *et al.* [CLAS Collaboration], Phys. Rev. C **78**, 045209 (2008).
 - [3] T. Barnes and F. E. Close, Phys. Lett. B **123**, 89 (1983); E. Golowich, E. Haqq, and G. Karl, Phys. Rev. D **28**, 160 (1983); C.E. Carlson and T.H. Hansson, Phys. Lett. B **128**, 95 (1983); I. Duck and E. Umland, Phys. Lett. B **128** (1983) 221.
 - [4] I. G. Aznauryan *et al.* [CLAS Collaboration], Phys. Rev. C **80**, 055203 (2009).
 - [5] I. G. Aznauryan and V. D. Burkert, Prog. Part. Nucl. Phys. **67**, 1 (2012).
 - [6] S. Capstick and P. R. Page, Phys. Rev. C **66**, 065204 (2002); Phys. Rev. D **60**, 111501 (1999).
 - [7] P. R. Page, Int. J. Mod. Phys. A **20**, 1791 (2005).
 - [8] C. K. Chow, D. Pirjol and T. M. Yan, Phys. Rev. D **59**, 056002 (1999).
 - [9] C. E. Carlson and N. C. Mukhopadhyay, Phys. Rev. Lett. **67**, 3745 (1991).
 - [10] T. T. Takahashi and H. Suganuma, Phys. Rev. Lett. **90**, 182001 (2003).
 - [11] J. J. Dudek and R. G. Edwards, Phys. Rev. D **85**, 054016 (2012).
 - [12] E. Kou, Phys. Rev. D **63**, 054027 (2001).
 - [13] For details see: <https://www.jlab.org/Hall-B/clas12-web/>
 - [14] Z. P. Li, Phys. Rev. D **44**, 2841 (1991).
 - [15] Z. P. Li, V. Burkert and Z. J. Li, Phys. Rev. D **46**, 70 (1992).
 - [16] C. Wu, J. Barth, W. Braun, J. Ernst, K. H. Glander, J. Hannappel, N. Jopen and H. Kalinowsky *et al.*, Eur. Phys. J. A **23**, 317 (2005).
 - [17] L. De Cruz, J. Ryckebusch, T. Vrancx and P. Vancraeyveld, Phys. Rev. C **86**, 015212 (2012).
 - [18] T. Corthals, D. G. Ireland, T. Van Cauteren and J. Ryckebusch, Phys. Rev. C **75**, 045204 (2007).
 - [19] A. Afanasev, I. Akushevich, V. Burkert and K. Joo, Phys. Rev. D **66**, 074004 (2002).
 - [20] K. Park *et al.* [CLAS Collaboration], Phys. Rev. C **91**, 045203 (2015).
 - [21] M. Ripani, V. Mokeev, M. Anghinolfi, M. Battaglieri, G. Fedotov, E. Golovach, B. Ishkhanov and M. Osipenko *et al.*, Nucl. Phys. A **672**, 220 (2000).
 - [22] I. G. Aznauryan, V. D. Burkert, G. V. Fedotov, B. S. Ishkhanov and V. I. Mokeev, Phys. Rev. C **72**, 045201 (2005).
 - [23] V. I. Mokeev *et al.*, in “Proc. of the Workshop on the Physics of Excited Nucleon. NSTAR2005”, ed. by S. Capstick, V. Crede, P. Eugenio, World Scientific Publishing Co., p. 47.
 - [24] V. I. Mokeev, V. D. Burkert, T. S. H. Lee, L. Elouadrhiri, G. V. Fedotov and B. S. Ishkhanov, Phys. Rev. C **80**, 045212 (2009).
 - [25] M. Ripani *et al.* [CLAS Collaboration], Phys. Rev. Lett. **91**, 022002 (2003)
 - [26] V. I. Mokeev *et al.* [CLAS Collaboration], Phys. Rev. C **86**, 035203 (2012)
 - [27] G. V. Fedotov *et al.* [CLAS Collaboration], Phys. Rev. C **79**, 015204 (2009)
 - [28] E. Golovach *et al.*, $\gamma p \rightarrow p\pi^+\pi^-$ cross sections from g11a experiment, CLAS ANALYSIS NOTE (in preparation).
 - [29] T. Vrancx, J. Ryckebusch and J. Nys, Phys. Rev. C **89**, no. 6, 065202 (2014)
 - [30] The StrangeCalc web-site <http://rprmodel.ugent.be/calc/>
 - [31] V. I. Mokeev *et al.*, Phys. Rev. C **80**, 022002 (2009).
 - [32] D. Luke and P. Soding, Multiple Pion Photoproduction in the s Channel Resonance Region, Springer Tracts in Modern Physics 59 (1971).
 - [33] E. Amaldi, S. Fubini and G. Furlan, Pion Electroproduction. Springer Tracts in Modern Physics **83**, ed. by G. Hohler (Springer Verlag, Berlin 1979).